Joint Beamforming Design for Double Active RIS-Assisted Radar-Communication Coexistence Systems

Mengyu Liu, Hong Ren, *Member, IEEE*, Cunhua Pan, *Senior Member, IEEE*, Boshi Wang, Zhiyuan Yu, Ruisong Weng, Kangda Zhi, and Yongchao He

***Abstract*—Integrated sensing and communication (ISAC) technology has been considered as one of the key candidate technologies in the next-generation wireless communication systems. However, when radar and communication equipment coexist in the same system, i.e., radar-communication coexistence (RCC), the interference from communication systems to radar can be large and cannot be ignored. Recently, reconfigurable intelligent surface (RIS) has been introduced into RCC systems to reduce the interference. However, the "multiplicative fading" effect introduced by passive RIS limits its performance. To tackle this issue, we consider a double active RIS-assisted RCC system, which focuses on the design of the radar's beamforming vector and the active RISs' reflecting coefficient matrices, to maximize the achievable data rate of the communication system. The considered system needs to meet the radar detection constraint and the power budgets at the radar and the RISs. Since the problem is non-convex, we propose an algorithm based on the penalty dual decomposition (PDD) framework. Specifically, we initially introduce auxiliary variables to reformulate the coupled variables into equation constraints and incorporate these constraints into the objective function through the PDD framework. Then, we decouple the equivalent problem into several subproblems by invoking the block coordinate descent (BCD) method. Furthermore, we employ the Lagrange dual method to alternately optimize these subproblems. Simulation results verify the effectiveness of the proposed algorithm. Furthermore, the results also show that under the same power budget, deploying double active RISs in RCC systems can achieve higher data rate than those with single active RIS and double passive RISs.**

***Index Terms*—Active reconfigurable intelligent surface (RIS), integrated sensing and communication (ISAC), radar-communication coexistence (RCC), penalty dual decomposition (PDD) algorithm.**

I. Introduction

NEXT-GENERATION wireless communication systems are expected to provide 100 times higher connection density compared with the fifth generation (5G) wireless communication system to support diverse communication scenarios [1]. However, the existence of a large number of devices aggravates the demand for wireless spectrum resources. To satisfy the demand, integrated sensing and communication (ISAC) technology has been advocated to share the frequency bandwidth with radar systems [2], [3]. Specifically, this technology can integrate the communication system and radar system by sharing frequency band resources, transmission waveforms, and hardware platforms. Therefore, ISAC can effectively reduce the hardware cost and improve the spectral and energy efficiencies.

There are two main implementation approaches for ISAC [4]: the radar-communication coexistence (RCC) system and the dual-functional radar and communication (DFRC) system. For the former, the hardware parts of the radar and the communication system are separate [5], while for the latter the hardware parts of the radar and the communication system are integrated [4]. Compared with DFRC systems, RCC systems typically refrain from altering the existing hardware structure and only consider the design of resource allocation strategies. With this in mind, RCC systems have attracted considerable interest [6]. However, the interference between radar and communication equipment can seriously degrade the achievable data rate of the communication system due to the coexistence. Recently, many researchers have made extensive contributions on the RCC systems to reduce the interference between communication systems and radar. By negotiating the spectrum use, the authors of [7] proposed the idea of cooperation between radar and communication systems to mitigate mutual interference while fulfilling power and rate constraints. In addition, the authors of [8] proposed an optimization algorithm based on the gradient projection method to solve the power minimization problem by exploiting the constructive multiuser interference.

Manuscript received 7 February 2024; revised 15 June 2024; accepted 30 July 2024. Date of publication 5 August 2024; date of current version 8 October 2024. The work of Hong Ren was supported in part by the National Natural Science Foundation of China under Grants 62350710796 and the Fundamental Research Funds for the Central Universities under Grant 2242022k60001. The work of Cunhua Pan was supported in part by the National Natural Science Foundation of China under Grants 62201137 and 62331023 and in part by the National Natural Science Foundation of China under Grants 62350710796 and the Fundamental Research Funds for the Central Universities under Grant 2242022k60001. The associate editor coordinating the review of this article and approving it for publication was S. Communication. *(Corresponding authors: Hong Ren; Cunhua Pan.)*

Mengyu Liu, Hong Ren, Cunhua Pan, Boshi Wang, Zhiyuan Yu, Ruisong Weng, and Yongchao He are with the National Mobile Communications Research Laboratory, Southeast University, Nanjing 210096, China (e-mail: mengyuliu@seu.edu.cn; hren@seu.edu.cn; cpan@seu.edu.cn; boshi_wang@seu.edu.cn; zyyu@seu.edu.cn; ruisong_weng@seu.edu.cn; heyongchao@seu.edu.cn).

Kangda Zhi is with the School of Electrical Engineering and Computer Science, Technical University of Berlin, 10623 Berlin, Germany (e-mail: k.zhi@tu-berlin.de).

Digital Object Identifier 10.1109/TCCN.2024.3438350

Recently, some works have deployed reconfigurable intelligent surface (RIS) in RCC systems to increase the degrees-of-freedom (DoFs) for designing the transmission strategy. Specifically, RISs are programmable meta-surfaces comprising multiple passive reflecting elements, each of which introduces a tunable phase shift to the incident signal. By controlling these reflecting elements, the signals reaching the intended receiver can be enhanced, while those reaching the unintended receiver can be suppressed [9], [10]. Therefore, RISs are endowed with the ability to customize the wireless channel and thus enhance the signal transmission, which enables its extensive application in wireless communications [11], [12]. Inspired by this, some researchers have already introduced the RIS into RCC systems to eliminate the interference between the communication systems and the radar [13], [14], [15]. The authors of [13] first proposed the concept of deploying single RIS in RCC systems for enhancing the detection probability of radar. In [14], the authors jointly designed the phase shift matrix of RIS and the precoding of base station (BS) with maximizing the communication data rate, which effectively reduces the interference between the communication system and the radar. Unlike the single RIS-assisted RCC system considered in [13] and [14], the authors of [15] deployed two RISs in RCC systems to eliminate the interference between radar and communication systems, which demonstrates that due to the RIS cooperation gain, deploying double RISs in RCC systems leads to better system performance than that of single RIS.

However, the gain of passive RIS is limited due to the fact that the signal reflected through the RIS suffers from double pathloss, resulting in severe attenuation at the receiver. This effect is called "multiplicative fading" [16], [17]. Fortunately, the concept of active RIS is proposed to overcome these limitations introduced by passive RIS [18], [19], [20]. Different from passive RIS, active RIS is equipped with an integrated active amplifier on each reflective element to compensate for signal attenuation, so that the gain of RIS can be fully unleashed. Additionally, the authors of [21] demonstrated that the active RIS could still improve the system performance compared to the passive RIS under the same power budget. Motivated by this, researchers have introduced active RIS into DFRC systems [22], [23], [24]. In [22], an active RIS was deployed in DFRC systems to enhance radar sensing performance and communication quality. Simulation results of [22] demonstrated the advantages of deploying active RIS in DFRC systems compared to passive RIS. The authors of [23] focused on an active RIS assisted DFRC system in the scenario of cloud radio access network (C-RAN) to generate some reflected beams directed from active RIS to the targets which were located in the non-line-of-sight area of remote radio heads (RRHs). Moreover, in [24], active RIS was applied to improve physical layer security in DFRC systems. These literature validated the superiority of active RIS over passive RIS in DFRC systems. However, the above works only focused on DFRC scenarios with a single active RIS. To the best of the authors' knowledge, the active RIS-aided RCC systems have not been studied, which is also an important application scenario for ISAC. Besides, considering the promising cooperative gain between double active RISs, the investigation of double active RIS-aided RCC systems is of significant importance and it is expected to achieve superior performance.

Therefore, in this paper, we investigate a double active RIS-assisted RCC system. Due to the presence of active RIS, the amplification of thermal noise and the power constraints of active RIS need to be considered, which means that the methods proposed by [13] and [15] cannot be directly applied. Meanwhile, the deployment of double RISs also introduces non-trivial challenges for the beamforming design. To tackle these challenges, we propose a low-complexity algorithm to solve the formulated optimization problem. The main contributions of this paper are summarized as follows:

1) To the best of our knowledge, this is the first attempt to investigate double active RIS-assisted RCC systems. By optimizing the radar's beamforming vector and the active RISs' reflecting coefficient matrices, we formulate the optimization problem that maximizes the achievable data rate of the communication system subject to the radar detection constraint and the power budgets at the radar and the RISs.
2) Then, we propose a low complexity algorithm based on the penalty dual decomposition (PDD) framework, which transforms the original problem into a more tractable form. In the inner loop, the problem can be divided into several subproblems using the block coordinate descent (BCD) method and each subproblem can be solved by using the Lagrange dual method. In the external loop, the dual and penalty parameters are updated. By utilizing our proposed low-complexity algorithm, the computational speed for identifying the optimal solution can be significantly enhanced.
3) To draw more insights, we derive a two-loop algorithm based on the PDD framework for the double passive RIS-assisted RCC system as a benchmark scheme. Different from active RIS, passive RIS introduces a unit-modulus constraint. To tackle this issue with low complexity, we use the Minorize-Maximization (MM) algorithm to optimize the phase shift matrix of passive RIS.
4) Finally, our simulation results reveal the advantages of the proposed scheme. We demonstrate that double active RISs can achieve much higher data rate than single active RIS and double passive RISs under the same power budget and the same number of reflecting elements. In addition, we verify the convergence and effectiveness of the proposed algorithm.

The remainder of this paper is organized as follows. In Section II, we present the system model and formulate the achievable data rate maximization problem. In Section III, a PDD-based algorithm is proposed to solve this problem. In Section IV, a benchmark algorithm based on passive RIS is derived. Finally, Sections V and VI provide the numerical results and conclusions, respectively.

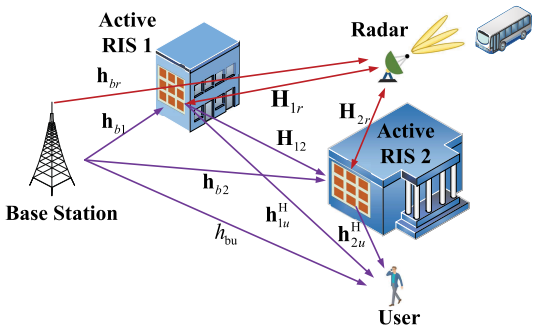

Fig. 1. Double active RIS-assisted radar-communication coexistence system.

Notations: In this paper, lowercase, boldface lowercase, and boldface uppercase letters are used to represent scalars, vectors and matrices, respectively. $\mathbf{I}$ and $\mathbf{0}$ denote an identity matrix and an all-zero vector, respectively. $\mathbb{C}^{M\times N}$ denotes the complex matrix whose dimension is $M \times N$. $\mathbb{E}\{\cdot\}$ denotes the operation of expectation. $\mathrm{diag}(\cdot)$ denotes the operation of diagonalization. Also, $\mathrm{blkdiag}(\cdot)$ denotes a block diagonal matrix. $|a|$ and $\mathrm{Re}(a)$ denote the absolute value, the real value of the complex number a. $\|\mathbf{a}\|_2$ is the 2-norm of vector $\mathbf{a}$. For matrix $\mathbf{A}$, Tr($\mathbf{A}$) and $\|\mathbf{A}\|_F$ denote the trace operation of $\mathbf{A}$ and Frobenius norm of $\mathbf{A}$, respectively. For two matrices $\mathbf{A}$ and $\mathbf{B}$, $\mathbf{A}\odot\mathbf{B}$ is used to denote the Hadamard product. $\mathcal{CN}(\mathbf{0},\mathbf{I})$ denotes a vector that follows a normal distribution with zero mean and unit covariance matrix. The conjugate, transpose and Hermitian operators are represented by $(\cdot)^*$, $(\cdot)^{\mathrm{T}}$ and $(\cdot)^{\mathrm{H}}$, respectively.

II. System Model and Problem Formulation

As shown in Fig. 1, we consider a double active RIS-assisted RCC system,[1] which consists of a pair of single-antenna BS and single-antenna user (UE) and a multiple-input multiple-output (MIMO) radar with M antennas, which can detect point-like targets in K directions within one detection epoch. Additionally, two active RISs named as active RIS 1 and active RIS 2 are deployed in this system. Without loss of generality, we assume that the active RIS 1 and active RIS 2 are equipped with N_1 and N_2 reflecting elements, respectively.

[1]We assume that the BS, radar and two RISs are all connected to the same central controller, which provides the channel state information (CSI). The required CSI can be obtained by some efficient channel estimation algorithms [25], [26].

A. Radar Model

We assume that the radar mainly detects potential targets in some directions. The K directions during one detection epoch are given by $\{\theta_k\}$, $\forall k \in \mathcal{K} \triangleq \{1,2,\ldots,K\}$. T is used to represent the pulse repetition interval (PRI). In addition, we assume that the probing signal is transmitted by radar at time t, and the echo signal is received from the targets at time t_0. Therefore, the probing signal transmitted by radar can be expressed as

$$\mathbf{x}[t] = \begin{cases} \mathbf{w}_k s_k, & t = (k-1)T, \forall k \in \mathcal{K}, \\ \mathbf{0}, & t \neq (k-1)T, \forall k \in \mathcal{K}. \end{cases} \tag{1}$$

where s_k and $\mathbf{w}_k \in \mathbb{C}^{M\times 1}$ denote the radar sensing symbols and the transmitting beamforming vector for direction $\theta_k, \forall k \in \mathcal{K}$, respectively. Specifically, we assume that s_k is an independent Gaussian random symbol with zero mean and unit signal power, i.e., $\mathbb{E}[s_i s_j^*] = 0, i \neq j$, and $\mathbb{E}[s_k s_k^*] = 1$.

Let $\mathbf{h}_{br} \in \mathbb{C}^{M\times 1}$, $\mathbf{h}_{b1} \in \mathbb{C}^{N_1\times 1}$, $\mathbf{H}_{1r} \in \mathbb{C}^{M\times N_1}$, and $\mathbf{H}_{2r} \in \mathbb{C}^{M\times N_2}$ denote the wireless channel for BS $\rightarrow$ radar, BS $\rightarrow$ active RIS 1, active RIS 1 $\rightarrow$ radar, and active RIS2 $\rightarrow$ radar, respectively. Specifically, $\rho_{i,n_i} e^{\varphi_{i,n_i}}$ denotes the reflecting coefficient of the n-th reflecting element of the i-th active RIS, where $\rho_{i,n_i} > 1$ and $\varphi_{i,n_i} \in [0, 2\pi]$. Then, the reflecting coefficient matrix of the i-th active RIS is $\mathbf{\Theta}_i = \mathrm{diag}(\boldsymbol{\phi}_i)$, where $\boldsymbol{\phi}_i \triangleq [\rho_{i,1_i} e^{\varphi_{i,1_i}}, \ldots, \rho_{i,N_i} e^{\varphi_{i,N_i}}]^{\mathrm{T}}, i \in \{1,2\}$.

The signal received by radar from the target in direction θ_k can be expressed as (2), as shown at the bottom of the page, where $\mathbf{A}_k \triangleq \alpha_k \mathbf{a}(\theta_k)\mathbf{a}^{\mathrm{H}}(\theta_k) \in \mathbb{C}^{M\times M}$ is the target response matrix for the direction θ_k. α_k denotes the pathloss factor of the target from direction θ_k and $\mathbf{a}(\theta_k) \triangleq [1, e^{j\frac{2\pi d}{\lambda}\sin\theta_k}, \ldots, e^{j\frac{2\pi d}{\lambda}(M-1)\sin\theta_k}]^{\mathrm{T}}$ is the array response vector of the radar antennas, where d and λ denotes the antenna spacing and the signal wavelength, respectively. Moreover, $c[t]$ and $P_{\mathrm{t}}^{\mathrm{act}}$ denote the communication signal from BS and the transmitted power at BS, $\mathbf{n}[t]$ denotes the thermal noise at the radar, which follows the distributions of $\mathbf{n}[t] \sim \mathcal{CN}(\mathbf{0}, \sigma^2\mathbf{I}_M)$. Note that, different from the passive RIS, the active RIS is equipped with an integrated active reflection-type amplifier, which is able to amplify the received signal by consuming additional power [27], [28]. According to the principle of the amplifier, the thermal noise at the input port is also amplified, causing interference that cannot be ignored.

$$\begin{aligned}\mathbf{y}_k^{\mathrm{r}}[t] = & \underbrace{\mathbf{A}_k\mathbf{x}[t-t_0]}_{\text{Echo signal from the target}} + \underbrace{(\mathbf{H}_{1r}\mathbf{\Theta}_1 + \mathbf{H}_{2r}\mathbf{\Theta}_2\mathbf{H}_{12}\mathbf{\Theta}_1)\mathbf{n}_1[t] + \mathbf{H}_{2r}\mathbf{\Theta}_2\mathbf{n}_2[t] + \mathbf{n}[t]}_{\text{Thermal nosie}} \\ & + \underbrace{\sum_{m=1,m\neq k}^{K} \mathbf{A}_m\mathbf{x}[t-t_0]}_{\text{Interference from other targets}} + \underbrace{(\mathbf{h}_{br} + \mathbf{H}_{1r}\mathbf{\Theta}_1\mathbf{h}_{b1} + \mathbf{H}_{2r}\mathbf{\Theta}_2\mathbf{h}_{b2} + \mathbf{H}_{2r}\mathbf{\Theta}_2\mathbf{H}_{12}\mathbf{\Theta}_1\mathbf{h}_{b1})\sqrt{P_{\mathrm{t}}^{\mathrm{act}}}c[t]}_{\text{Interference from BS to radar}},\end{aligned} \tag{2}$$

$$\mathrm{SINR}_k^{\mathrm{r}} = \frac{\left|\mathbf{d}_k^{\mathrm{H}}\mathbf{A}_k\mathbf{w}_k\right|^2}{\sum_{m=1,m\neq k}^{K}\left|\mathbf{d}_k^{\mathrm{H}}\mathbf{A}_m\mathbf{w}_k\right|^2 + P_{\mathrm{t}}^{\mathrm{act}}\left|\mathbf{d}_k^{\mathrm{H}}\mathbf{q}\right|^2 + \sigma_1^2\left\|\mathbf{d}_k^{\mathrm{H}}\mathbf{B}\right\|_2^2 + \sigma_2^2\left\|\mathbf{d}_k^{\mathrm{H}}\mathbf{C}\right\|_2^2 + \sigma^2\left\|\mathbf{d}_k^{\mathrm{H}}\right\|_2^2}, \tag{3}$$

Furthermore, the received beamforming vector $\mathbf{d}_k^{\mathrm{H}} \in \mathbb{C}^{1\times M}$ is used to detect the echo signal from the direction θ_k. Thus, by defining the equivalent channel matrices $\mathbf{B} \triangleq \mathbf{H}_{2r}\mathbf{\Theta}_2\mathbf{H}_{12}\mathbf{\Theta}_1 + \mathbf{H}_{1r}\mathbf{\Theta}_1 \in \mathbb{C}^{M\times N_1}$, $\mathbf{C} \triangleq \mathbf{H}_{2r}\mathbf{\Theta}_2 \in \mathbb{C}^{M\times N_2}$, and $\mathbf{q} \triangleq \mathbf{h}_{br} + \mathbf{B}\mathbf{h}_{b1} + \mathbf{C}\mathbf{h}_{b2} \in \mathbb{C}^{M\times 1}$, the radar signal-to-interference-plus-noise ratio (SINR)[2] in terms of the direction θ_k can be expressed as (3), as shown at the bottom of the previous page.

B. Communication Model

Let h_{bu}, $\mathbf{h}_{b1} \in \mathbb{C}^{N_1\times 1}$, $\mathbf{h}_{b2} \in \mathbb{C}^{N_2\times 1}$, $\mathbf{H}_{12} \in \mathbb{C}^{N_2\times N_1}$, $\mathbf{h}_{2u}^{\mathrm{H}} \in \mathbb{C}^{1\times N_2}$, $\mathbf{h}_{1u}^{\mathrm{H}} \in \mathbb{C}^{1\times N_1}$ denote the wireless channel for BS $\rightarrow$ UE, BS $\rightarrow$ active RIS 1, active RIS 1 $\rightarrow$ active RIS 2, active RIS 2 $\rightarrow$ UE, and active RIS 1 $\rightarrow$ UE, respectively. Then, the received signal at the user at the time t can be expressed as (4), as shown at the bottom of next page, where $n_0[t]$ and $\mathbf{n}_i[t]$ are the thermal noise at the user and the i-th active RIS, respectively, following the distributions of $n_0[t] \sim \mathcal{CN}(0, \sigma_0^2)$, and $\mathbf{n}_i[t] \sim \mathcal{CN}(\mathbf{0}, \sigma_i^2\mathbf{I}_{N_i})$.

Note that, as shown in Fig. 1, the targets of interest are not located near active RIS since active RIS is usually deployed on the facade of tall buildings. In addition, when the number of radar antennas is large, the radar beam is usually narrow, making it less likely to interfere with the communication system. Furthermore, the interference from radar to user can also be reduced using some techniques such as [30], [31]. Therefore, radar interference to users is likely to be small and will not be considered in this paper.

Based on the above discussions, the communication signal to noise ratio (SNR) for the user during one detection epoch can be expressed as (5), as shown at the bottom of next page. Then, the achievable data rate (bit/s/Hz) is given by

$$R = \log_2(1 + \mathrm{SNR}^{\mathrm{c}}). \tag{6}$$

Furthermore, since the active RIS is equipped with integrated active amplifiers, the thermal noise on the active RIS will also be amplified by the same factors as the transmitted signal. Moreover, the existence of active amplifiers leads to extra power consumption [18]. Recall that, the reflecting coefficient matrix of the i-th active RIS is discussed in the last section, the power constraints of active RIS 1 and active RIS 2 can be expressed as follows

$$\|\mathbf{\Theta}_1\mathbf{h}_{b1}\|_2^2 + \sigma_1^2\|\mathbf{\Theta}_1\|_F^2 \le P_1, \tag{7a}$$

$$\|\mathbf{\Theta}_2\mathbf{H}_{12}\mathbf{\Theta}_1\mathbf{h}_{b1}\|_2^2 + \|\mathbf{\Theta}_2\mathbf{h}_{b2}\|_2^2 + \sigma_1^2\|\mathbf{\Theta}_2\mathbf{H}_{12}\mathbf{\Theta}_1\|_F^2 + \sigma_2^2\|\mathbf{\Theta}_2\|_F^2 \le P_2, \tag{7b}$$

where P_1 and P_2 denote the power budgets of active RIS 1 and active RIS 2, respectively.

C. Problem Formulation

In this paper, we aim to maximize the achievable data rate of the communication system by jointly optimizing the radar transmit beamforming vector $\{\mathbf{w}_k\}$, radar receive beamforming vector $\{\mathbf{d}_k\}$, and the reflecting coefficient matrices $\mathbf{\Theta}_1$ and $\mathbf{\Theta}_2$ of two active RISs while guaranteeing the SINR of radar for each detecting direction $\{\theta_k\}$ and power limitation of radar and two active RISs. Hence, the optimization problem is formulated as

$$\max_{\substack{\{\mathbf{w}_k\},\{\mathbf{d}_k\},\\ \mathbf{\Theta}_1,\mathbf{\Theta}_2}} \quad R \tag{8a}$$

$$\text{s.t.} \quad \mathrm{SINR}_k^{\mathrm{r}} \ge \eta, \forall k \in \mathcal{K}, \tag{8b}$$

$$\sum_{k=1}^{K} \|\mathbf{w}_k\|_2^2 \le P_{\mathrm{r}}, \tag{8c}$$

$$\text{(7a)}, \ \text{(7b)},$$

where η and P_{r} denote the SINR requirement and the power budget for the radar, respectively. Constraint (8b) denotes the minimum SINR requirement to ensure the detection accuracy of radar. Constraint (8c) guarantees the power budget of radar.

However, the strong couplings among variables $\mathbf{w}_k$, $\mathbf{d}_k$, $\mathbf{\Theta}_1$, and $\mathbf{\Theta}_2$ and constraint (8b) make Problem (8) particularly challenging to solve. Therefore, we will develop a low-complexity algorithm based on PDD framework to solve this problem in the following section.

III. Joint Beamforming Design Algorithm for Active RIS

In this section, we first reformulate the original problem into a more feasible form by using fractional programming (FP) method. Then, to tackle the coupling of these variables. We create some equality constraints and integrated into the objective function by using PDD algorithm. After that, we adopt the concave-convex procedure (CCP) method to tackle the non-convex property of the constraints. Finally, the BCD algorithm is used to divide the problem into several subproblems. Each subproblem is solved by using the Lagrange dual method.

A. Reformulation of the Original Problem

Notice that the achievable data rate increases as the communication SNR increases. Therefore, in the following sections, we can replace the objective function of the original problem, i.e., R with the communication SNR, i.e., $\mathrm{SNR}^{\mathrm{c}}$. Furthermore, in order to efficiently solve the optimization problem with a fractional objective function, we introduce an auxiliary x and apply the quadratic transformation of the FP method [32]. As a result, we can find a lower bound for $\mathrm{SNR}^{\mathrm{c}}$ which can be expressed as

$$\begin{aligned}\tilde{f}(\mathbf{\Theta}_1,\mathbf{\Theta}_2,x) \triangleq\ & |x|^2(\sigma_1^2\left\|\mathbf{h}_{2u}^{\mathrm{H}}\mathbf{\Theta}_2\mathbf{H}_{12}\mathbf{\Theta}_1 + \mathbf{h}_{1u}^{\mathrm{H}}\mathbf{\Theta}_1\right\|_2^2 \\ & + \sigma_2^2\left\|\mathbf{h}_{2u}^{\mathrm{H}}\mathbf{\Theta}_2\right\|_2^2 + \sigma_0^2) \\ & - 2\mathrm{Re}\Big\{x^*\sqrt{P_{\mathrm{t}}^{\mathrm{act}}}\Big(h_{\mathrm{bu}} + \mathbf{h}_{1u}^{\mathrm{H}}\mathbf{\Theta}_1\mathbf{h}_{b1} \\ & + \mathbf{h}_{2u}^{\mathrm{H}}\mathbf{\Theta}_2\mathbf{H}_{12}\mathbf{\Theta}_1\mathbf{h}_{b1} + \mathbf{h}_{2u}^{\mathrm{H}}\mathbf{\Theta}_2\mathbf{h}_{b2}\Big)\Big\}. \end{aligned} \tag{9}$$

[2]The SINR commonly serves as a key metric for measuring sensing performance [22], [29], and is closely associated with the Kullback-Leibler (KL) divergences. Besides, the interference from the active RIS may degrade the sensing performance. Therefore, for ease of analysis, we use the SINR to measure the radar's sensing performance.

Then, the relationship between $\mathrm{SNR}^{\mathrm{c}}$ and $f(\boldsymbol{\Theta}_1, \boldsymbol{\Theta}_2, x)$ can be written as

$$\mathrm{SNR}^{\mathrm{c}} = \max_{x} \quad \tilde{f}(\boldsymbol{\Theta}_1, \boldsymbol{\Theta}_2, x), \tag{10}$$

where the optimal solution x^{opt} can be represented by (11), shown at the bottom of the page. Thus, we rewrite Problem (8) as follows

$$\begin{aligned} \mathcal{P}_1 : \min_{\substack{\{\mathbf{w}_k\},\{\mathbf{d}_k\},\boldsymbol{\Theta}_1,\\ \boldsymbol{\Theta}_2,x}} \quad & \tilde{f}(\boldsymbol{\Theta}_1, \boldsymbol{\Theta}_2, x), \\ \text{s.t.} \quad & \text{(8b), (8c), (7a), (7b).} \end{aligned} \tag{12}$$

However, there is a non-linear coupling of variables in constraint (8b), which makes Problem (12) difficult to solve. Therefore, in the following sections, we adopt the PDD algorithm to tackle this issue.

B. The Penalty Dual Decomposition (PDD) Algorithm for the Outer Loop

The PDD algorithm is a two-loop iterative algorithm that can effectively solve non-convex optimization problems, especially in the case of non-linear coupling of optimization variables. The inner loop of the PDD algorithm solves the lagrangian problem, while the outer loop iterates over the penalty and dual parameters until it converges [33].

According to the Problem (12), non-convexity property of constraint (8b) and the non-linear couplings between these variables in constraint cannot directly solve by the existing methods. Therefore, we adopt the PDD algorithm to solve this problem. Specifically, we first create some equality constraints. Then, these equality constraints can be treated as penalty terms and integrated into objective function by using the PDD algorithm.

In order to tackle the coupling of variables in constraint (8b), we introduce the auxiliary variables $\{u_k, v_k, y_k, \mathbf{e}_k, \mathbf{t}_k\}$, the equality constraints associated with five auxiliary variables are as follows

$$u_k - \mathbf{d}_k^{\mathrm{H}} \mathbf{A}_k \mathbf{w}_k = 0, \forall k \in \mathcal{K}, \tag{13a}$$
$$v_k - \mathbf{d}_k^{\mathrm{H}} \mathbf{q} = 0, \forall k \in \mathcal{K}, \tag{13b}$$
$$y_k - \sum_{m=1, m\neq k}^{K} \mathbf{d}_k^{\mathrm{H}} \mathbf{A}_m \mathbf{w}_k = 0, \forall k \in \mathcal{K}, \tag{13c}$$
$$\mathbf{e}_k^{\mathrm{H}} - \mathbf{d}_k^{\mathrm{H}} \mathbf{B} = \mathbf{0}, \forall k \in \mathcal{K}, \tag{13d}$$
$$\mathbf{t}_k^{\mathrm{H}} - \mathbf{d}_k^{\mathrm{H}} \mathbf{C} = \mathbf{0}, \forall k \in \mathcal{K}. \tag{13e}$$

Next, we substitute the auxiliary variables into constraint (8b). The new constraint (8b) can therefore be written as

$$\eta\Big(|y_k|^2 + P_{\mathrm{t}}^{\mathrm{act}} |v_k|^2 + \sigma_1^2 \left\| \mathbf{e}_k^{\mathrm{H}} \right\|_2^2 + \sigma_2^2 \left\| \mathbf{t}_k^{\mathrm{H}} \right\|_2^2 + \sigma^2 \left\| \mathbf{d}_k^{\mathrm{H}} \right\|_2^2 \Big) - |u_k|^2 \leq 0. \tag{14}$$

After introducing the equality constraints, we can solve Problem (12) using the PDD framework in the following section.

Based on the PDD framework, we can construct the following new objective function

$$\begin{aligned} \mathcal{P}_2 : \min_{\boldsymbol{\Omega}_1} \quad & \tilde{f}(\boldsymbol{\Theta}_1, \boldsymbol{\Theta}_2, x) + \frac{1}{2\rho} \sum_{k=1}^{K} \left| u_k - \mathbf{d}_k^{\mathrm{H}} \mathbf{A}_k \mathbf{w}_k + \rho \lambda_{k,1} \right|^2 \\ & + \frac{1}{2\rho} \sum_{k=1}^{K} \left| v_k - \mathbf{d}_k^{\mathrm{H}} \mathbf{q} + \rho \lambda_{k,2} \right|^2 \\ & + \frac{1}{2\rho} \sum_{k=1}^{K} \left| y_k - \mathbf{d}_k^{\mathrm{H}} \mathbf{A}_m \mathbf{w}_k + \rho \lambda_{k,3} \right|^2 \\ & + \frac{1}{2\rho} \sum_{k=1}^{K} \left\| \mathbf{e}_k^{\mathrm{H}} - \mathbf{d}_k^{\mathrm{H}} \mathbf{B} + \rho \boldsymbol{\lambda}_{k,\mathrm{e}}^{\mathrm{T}} \right\|_2^2 \\ & + \frac{1}{2\rho} \sum_{k=1}^{K} \left\| \mathbf{t}_k^{\mathrm{H}} - \mathbf{d}_k^{\mathrm{H}} \mathbf{C} + \rho \boldsymbol{\lambda}_{k,\mathrm{t}}^{\mathrm{T}} \right\|_2^2, \\ \text{s.t.} \quad & \text{(8c), (7a), (7b), (14),} \end{aligned} \tag{15}$$

where ρ is a penalty parameter, and $\{\lambda_{k,1}, \lambda_{k,2}, \lambda_{k,3}, \boldsymbol{\lambda}_{k,\mathrm{e}}^{\mathrm{T}} \boldsymbol{\lambda}_{k,\mathrm{t}}^{\mathrm{T}}\}$ are the dual parameters. $\boldsymbol{\omega}_1 \triangleq \{\mathbf{w}_k, \mathbf{d}_k, \boldsymbol{\Theta}_1, \boldsymbol{\Theta}_2, x, u_k, v_k, y_k, \mathbf{e}_k, \mathbf{t}_k\}$. Note that, when $\rho \to 0$, the solutions of Problem $\mathcal{P}_2$ are equal to those of Problem $\mathcal{P}_1$. Additionally, the convergence of the PDD algorithm was proved in [33].

$$\begin{aligned} \mathrm{y}^{\mathrm{c}}[t] = & \underbrace{\left(h_{\mathrm{bu}} + \mathbf{h}_{2u}^{\mathrm{H}} \boldsymbol{\Theta}_2 \mathbf{H}_{12} \boldsymbol{\Theta}_1 \mathbf{h}_{b1} + \mathbf{h}_{1u}^{\mathrm{H}} \boldsymbol{\Theta}_1 \mathbf{h}_{b1} + \mathbf{h}_{2u}^{\mathrm{H}} \boldsymbol{\Theta}_2 \mathbf{h}_{b2} \right) \sqrt{P_{\mathrm{t}}^{\mathrm{act}}} c[t]}_{\text{Communication signal from BS to user}} \\ & + \underbrace{\left(\mathbf{h}_{2u}^{\mathrm{H}} \boldsymbol{\Theta}_2 \mathbf{H}_{12} \boldsymbol{\Theta}_1 + \mathbf{h}_{1u}^{\mathrm{H}} \boldsymbol{\Theta}_1 \right) \mathbf{n}_1[t] + \mathbf{h}_{2u}^{\mathrm{H}} \boldsymbol{\Theta}_2 \mathbf{n}_2[t] + n_0[t]}_{\text{Thermal noise}} + \underbrace{\left((\mathbf{h}_{2u}^{\mathrm{H}} \boldsymbol{\Theta}_2 \mathbf{H}_{12} + \mathbf{h}_{1u}^{\mathrm{H}}) \boldsymbol{\Theta}_1 \mathbf{H}_{1r}^{\mathrm{H}} + \mathbf{h}_{2u}^{\mathrm{H}} \boldsymbol{\Theta}_2 \mathbf{H}_{2r}^{\mathrm{H}} \right) \mathbf{x}[t]}_{\text{Interference from radar to user}}, \end{aligned} \tag{4}$$

$$\mathrm{SNR}^{\mathrm{c}} = \frac{P_{\mathrm{t}}^{\mathrm{act}} \left| h_{\mathrm{bu}} + \mathbf{h}_{2u}^{\mathrm{H}} \boldsymbol{\Theta}_2 \mathbf{H}_{12} \boldsymbol{\Theta}_1 \mathbf{h}_{b1} + \mathbf{h}_{1u}^{\mathrm{H}} \boldsymbol{\Theta}_1 \mathbf{h}_{b1} + \mathbf{h}_{2u}^{\mathrm{H}} \boldsymbol{\Theta}_2 \mathbf{h}_{b2} \right|^2}{\sigma_1^2 \left\| \mathbf{h}_{2u}^{\mathrm{H}} \boldsymbol{\Theta}_2 \mathbf{H}_{12} \boldsymbol{\Theta}_1 + \mathbf{h}_{1u}^{\mathrm{H}} \boldsymbol{\Theta}_1 \right\|_2^2 + \sigma_2^2 \left\| \mathbf{h}_{2u}^{\mathrm{H}} \boldsymbol{\Theta}_2 \right\|_2^2 + \sigma_0^2}, \tag{5}$$

$$x^{\mathrm{opt}} = \frac{\sqrt{P_t^{act}} \left(h_{bu} + \mathbf{h}_{2u}^{\mathrm{H}} \boldsymbol{\Theta}_2 \mathbf{H}_{12} \boldsymbol{\Theta}_1 \mathbf{h}_{b1} + \mathbf{h}_{1u}^{\mathrm{H}} \boldsymbol{\Theta}_1 \mathbf{h}_{b1} + \mathbf{h}_{2u}^{\mathrm{H}} \boldsymbol{\Theta}_2 \mathbf{h}_{b2} \right)}{\sigma_1^2 \left(\left\| \mathbf{h}_{2u}^{\mathrm{H}} \boldsymbol{\Theta}_2 \mathbf{H}_{12} \boldsymbol{\Theta}_1 + \mathbf{h}_{1u}^{\mathrm{H}} \boldsymbol{\Theta}_1 \right\|_2^2 \right) + \sigma_2^2 \left\| \mathbf{h}_{2u}^{\mathrm{H}} \boldsymbol{\Theta}_2 \right\|_2^2 + \sigma_0^2} \tag{11}$$

However, since the constraint (14) is not convex, we need to use the CCP method to decompose this constraint [34]. To this end, the constraint (14) can be rewritten as

$$f(\mathbf{d}_k, v_k, y_k, \mathbf{e}_k, \mathbf{t}_k) - g(u_k) \leq 0, \forall k \in \mathcal{K}, \tag{16}$$

where

$$g(u_k) = |u_k|^2, \tag{17a}$$

$$f(\mathbf{d}_k, v_k, y_k, \mathbf{e}_k, \mathbf{t}_k) = \eta\Big(|y_k|^2 + P_{\mathrm{t}}^{\mathrm{act}}|v_k|^2 + \sigma_1^2\left\|\mathbf{e}_k^{\mathrm{H}}\right\|_2^2 + \sigma_2^2\left\|\mathbf{t}_k^{\mathrm{H}}\right\|_2^2 + \sigma^2\left\|\mathbf{d}_k^{\mathrm{H}}\right\|_2^2\Big). \tag{17b}$$

Then, we can approximate the convex function $g(u_k)$ in the i-th iteration by its first-order Taylor expansion near the point $u_k^{(i)}$, as

$$\hat{g}\left(u_k^{(i)}, u_k\right) = 2\mathrm{Re}\left((u_k^{(i)})^* u_k\right) - \left|u_k^{(i)}\right|^2. \tag{18}$$

Therefore, the constraint (14) can be approximated as

$$f(\mathbf{d}_k, v_k, y_k, \mathbf{e}_k, \mathbf{t}_k) - \hat{g}\left(u_k^{(i)}, u_k\right) \leq 0, \forall k \in \mathcal{K}. \tag{19}$$

Based on the above CCP method, we can recast Problem (8) as

$$\begin{aligned}\min_{\mathbf{\Omega}_1}\ & \tilde{f}(\mathbf{\Theta}_1, \mathbf{\Theta}_2, x) + \frac{1}{2\rho}\sum_{k=1}^{K}\left|u_k - \mathbf{d}_k^{\mathrm{H}}\mathbf{A}_k\mathbf{w}_k + \rho\lambda_{k,1}\right|^2 \\ &+ \frac{1}{2\rho}\sum_{k=1}^{K}\left|v_k - \mathbf{d}_k^{\mathrm{H}}\mathbf{q} + \rho\lambda_{k,2}\right|^2 \\ &+ \frac{1}{2\rho}\sum_{k=1}^{K}\left|y_k - \mathbf{d}_k^{\mathrm{H}}\mathbf{A}_m\mathbf{w}_k + \rho\lambda_{k,3}\right|^2 \\ &+ \frac{1}{2\rho}\sum_{k=1}^{K}\|\mathbf{e}_k^{\mathrm{H}} - \mathbf{d}_k^{\mathrm{H}}\mathbf{B} + \rho\boldsymbol{\lambda}_{k,\mathrm{e}}^{\mathrm{T}}\|_2^2 \\ &+ \frac{1}{2\rho}\sum_{k=1}^{K}\|\mathbf{t}_k^{\mathrm{H}} - \mathbf{d}_k^{\mathrm{H}}\mathbf{C} + \rho\boldsymbol{\lambda}_{k,\mathrm{t}}^{\mathrm{T}}\|_2^2, \\ \text{s.t.}\quad & \text{(8c), (7a), (7b), (19).}\end{aligned} \tag{20}$$

Note that Problem (20) can be readily verified as a convex problem, which can be solved by using CVX [35]. However, the computational complexity of using the CVX to solve Problem (20) is very high. To reduce the complexity, we next solve Problem (20) by using the Lagrange dual method.

C. The BCD Algorithm for the Inner Loop

In this subsection, we solve the augmented Lagrange (AL) problem using the BCD method [36]. We divide the optimization variables into eight blocks. The details of solving these subproblems are shown as follows.

1) Optimizing the Beamforming Vector $\mathbf{w}_k$: In this subproblem, we fix other variables to optimize $\mathbf{w}_k$. To simplify the formulation of Problem (20), we first define the following parameters

$$\mathbf{\Gamma}_k = \mathbf{A}_k^{\mathrm{H}}\mathbf{d}_k\mathbf{d}_k^{\mathrm{H}}\mathbf{A}_k + \sum_{m=1,m\neq k}^{K}\mathbf{A}_m^{\mathrm{H}}\mathbf{d}_k\mathbf{d}_k^{\mathrm{H}}\mathbf{A}_m, \tag{21a}$$

$$\mathbf{p}_k = \left(u_k + \rho\lambda_{k,1}\right)\mathbf{A}_k^{\mathrm{H}}\mathbf{d}_k + \left(y_k + \rho\lambda_{k,3}\right)\mathbf{A}_m^{\mathrm{H}}\mathbf{d}_k, \tag{21b}$$

$$\mathbf{\Gamma} = \mathrm{blkdiag}([\mathbf{\Gamma}_1, \ldots, \mathbf{\Gamma}_K]), \mathbf{p} = \left[\mathbf{p}_1^{\mathrm{T}}, \ldots, \mathbf{p}_K^{\mathrm{T}}\right]^{\mathrm{T}}. \tag{21c}$$

Then, Problem (20) can be reformulated as

$$\min_{\mathbf{w}}\ \mathbf{w}^{\mathrm{H}}\mathbf{\Gamma}\mathbf{w} - 2\mathrm{Re}\left\{\mathbf{p}^{\mathrm{H}}\mathbf{w}\right\}, \tag{22a}$$

$$\text{s.t.}\ \ \mathbf{w}^{\mathrm{H}}\mathbf{w} \leq P_{\mathrm{r}}, \tag{22b}$$

where $\mathbf{w} = [\mathbf{w}_1^{\mathrm{T}}, \ldots, \mathbf{w}_K^{\mathrm{T}}]^{\mathrm{T}}$. Since this subproblem (22) is a quadratic constraint quadratic programming (QCQP) problem, we can use the Lagrange multiplier method [37] to solve this problem. Then, the optimal solution $\mathbf{w}^{\mathrm{opt}}$ can be given by

$$\mathbf{w}^{\mathrm{opt}} = (\mathbf{\Gamma} + \mu\mathbf{I})^{-1}\mathbf{p}, \tag{23}$$

where $\mu \geq 0$ is the Lagrange multiplier which needs to satisfy the complementary slackness conditions for constraint (22b). Specifically, we can use the bisection search method [37] to obtain the optimal value of μ. The algorithm to solve Problem (22) is summarized in Algorithm 1.

Algorithm 1 Bisection Search Method to Solve Problem (22)

```
Initialize the accuracy ε, the bounds μ^lb and μ^ub;
repeat
  if Σ_{k=1}^K ||w^opt(0)||^2 ≤ P_r then
    Terminate;
  else
    continue;
  end if
  Compute μ = (μ^lb + μ^ub)/2;
  if Σ_{k=1}^K ||w^opt(μ)||^2 ≤ P_r then
    μ^ub = μ;
  else
    μ^lb = μ;
  end if
until |μ^lb − μ^ub| ≤ ε.
```

2) Optimizing the Receiving Beamforming Vector $\mathbf{d}_k$: In this block, we optimize $\mathbf{d}_k$ by fixing other variables. To simplify the representation, we first define the following parameters

$$\begin{aligned}\beth_k = {} & \mathbf{A}_k\mathbf{w}_k\mathbf{w}_k{}^{\mathrm{H}}\mathbf{A}_k^{\mathrm{H}} + \sum_{m=1,m\neq k}^{K}\mathbf{A}_m\mathbf{w}_k\mathbf{w}_k^{\mathrm{H}}\mathbf{A}_m^{\mathrm{H}} \\ & + \mathbf{q}\mathbf{q}^{\mathrm{H}} + \mathbf{B}\mathbf{B}^{\mathrm{H}} + +\mathbf{C}\mathbf{C}^{\mathrm{H}},\end{aligned} \tag{24a}$$

$$\begin{aligned}m = {} & \frac{1}{\sigma^2}\Big(\eta\Big(|y_k|^2 + P_{\mathrm{t}}^{\mathrm{act}}|v_k|^2 + \sigma_1^2\left\|\mathbf{e}_k^{\mathrm{H}}\right\|_2^2 \\ & + \sigma_2^2\left\|\mathbf{t}_k^{\mathrm{H}}\right\|_2^2\Big) - 2\mathrm{Re}((u_k^{(i)})^* u_k) + \left|u_k^{(i)}\right|^2\Big),\end{aligned} \tag{24b}$$

$$\begin{aligned}\mathbf{z}_k = {} & \left(u_k + \rho\lambda_{k,1}\right)\mathbf{A}_k\mathbf{w}_k + \left(v_k + \rho\lambda_{k,2}\right)\mathbf{q} \\ & + \left(y_k + \rho\lambda_{k,3}\right)\mathbf{A}_m\mathbf{w}_k + \mathbf{B}\left(\mathbf{e}_k^{\mathrm{H}} + \rho\boldsymbol{\lambda}_{k,\mathrm{e}}^{\mathrm{T}}\right) \\ & + \mathbf{C}\left(\mathbf{t}_k^{\mathrm{H}} + \rho\boldsymbol{\lambda}_{k,\mathrm{t}}^{\mathrm{T}}\right).\end{aligned} \tag{24c}$$

Then, Problem (20) can be reformulated as

$$\min_{\mathbf{d}_k}\ \mathbf{d}_k^{\mathrm{H}}\beth_k\mathbf{d}_k - 2\mathrm{Re}\left\{\mathbf{z}_k^{\mathrm{H}}\mathbf{d}_k\right\}, \tag{25a}$$

$$\text{s.t.}\ \ \mathbf{d}_k^{\mathrm{H}}\mathbf{d}_k \le m, \forall k \in \mathcal{K}. \tag{25b}$$

Next, we solve this subproblem (25) using the Lagrange dual method. The optimal solution $\mathbf{d}_k^{\mathrm{opt}}$ can be given by

$$\mathbf{d}_k^{\mathrm{opt}} = (\beth_k + \delta_k \mathbf{I}_M)^{-1}\mathbf{z}_k, \forall k \in \mathcal{K}, \tag{26}$$

where $\delta_k \ge 0$ is the Lagrange multiplier associated with constraint (25b) which can be found by the bisection search method.

3) Optimizing the Auxiliary Parameters: In this section, we alternately optimize the auxiliary parameters in $\{u_k, v_k, y_k, \mathbf{e}_k, \mathbf{t}_k\}$.

Firstly, we optimize $\{u_k\}$ while fixing other variables. Thus, original Problem (20) can be simplified as

$$\min_{u_k} \ \left|u_k - \mathbf{d}_k^{\mathrm{H}}\mathbf{A}_k\mathbf{w}_k + \rho\lambda_{k,1}\right|^2, \quad \text{s.t. (19).} \tag{27}$$

For this subproblem, we can use the Lagrangian dual method. Therefore, the optimal solution u_k^{opt} can be given by

$$u_k^{\mathrm{opt}} = \mathbf{d}_k^{\mathrm{H}}\mathbf{A}_k\mathbf{w}_k - \rho\lambda_{k,1} + \mu_k u_k^{(i)}, \forall k \in \mathcal{K}, \tag{28}$$

where $\mu_k \ge 0$ is the Lagrange multiplier associated with constraint (19) which can be found by the bisection search method.

It can be observed that the methods used in optimizing the variables $\{v_k, y_k, \mathbf{e}_k, \mathbf{t}_k\}$ are similar to optimizing u_k. Therefore, we can derive the optimal solutions for the remaining variables $v_k, y_{k,m}, \mathbf{e}_k^{\mathrm{H}}, \mathbf{t}_k^{\mathrm{H}}$ as

$$v_k^{\mathrm{opt}} = \frac{\mathbf{d}_k^{\mathrm{H}}\mathbf{q} - \rho\lambda_{k,2}}{1 + \varrho_k\eta P_{\mathrm{t}}^{\mathrm{act}}}, \forall k \in \mathcal{K}, \tag{29a}$$

$$y_k^{\mathrm{opt}} = \frac{\sum_{m=1,m\neq k}^{K}\mathbf{d}_k^{\mathrm{H}}\mathbf{A}_m\mathbf{w}_k - \rho\lambda_{k,3}}{1 + \zeta_k\eta}, \forall k \in \mathcal{K}, \tag{29b}$$

$$\mathbf{e}_k^{\mathrm{H}} = \frac{\mathbf{d}_k^{\mathrm{H}}\mathbf{B} - \rho\boldsymbol{\lambda}_{k,\mathrm{e}}^{\mathrm{T}}}{1 + \chi_k\eta\sigma_1^2}, \forall k \in \mathcal{K}, \tag{29c}$$

$$\mathbf{t}_k^{\mathrm{H}} = \frac{\mathbf{d}_k^{\mathrm{H}}\mathbf{C} - \rho\boldsymbol{\lambda}_{k,\mathrm{t}}^{\mathrm{T}}}{1 + \varsigma_k\eta\sigma_2^2}, \forall k \in \mathcal{K}, \tag{29d}$$

where $\varrho_k, \zeta_k, \chi_k, \varsigma_k \ge 0$ are the Lagrange multipliers associated with their corresponding constraints, and the values of these multipliers can be found by the bisection search method.

4) Optimizing the Phase Shift $\boldsymbol{\Theta}_1$: We optimize $\boldsymbol{\Theta}_1$ while fixing the other variables. To simplify the formulation of Problem (20), we first define $\mathbf{T}_1 = x^*\sqrt{P_{\mathrm{t}}^{\mathrm{act}}}\mathbf{H}_{12}^{\mathrm{H}}\boldsymbol{\Theta}_2^{\mathrm{H}}\mathbf{h}_{2u}\mathbf{h}_{b1}^{\mathrm{H}}$, $\mathbf{F}_1 \triangleq x^*\sqrt{P_{\mathrm{t}}^{\mathrm{act}}}\mathbf{h}_{1u}\mathbf{h}_{b1}^{\mathrm{H}}$, $\mathbf{S}_k = (\mathbf{H}_{2r}\boldsymbol{\Theta}_2\mathbf{H}_{12} + \mathbf{H}_{1r})^{\mathrm{H}}\mathbf{d}_k(\mathbf{e}_k + \rho\boldsymbol{\lambda}_{k,e})$. $\mathbf{t}_1$, $\mathbf{f}_1$, and $\mathbf{s}_k$ denote the collection of diagonal elements of matrix $\mathbf{T}_1$, $\mathbf{F}_1$ and $\mathbf{S}_k$, respectively.

By using the property $\mathrm{Tr}(\boldsymbol{\Theta}_1^{\mathrm{H}}\mathbf{D}_1\boldsymbol{\Theta}_1) = \boldsymbol{\phi}_1^{\mathrm{H}}(\mathbf{D}_1 \odot \mathbf{I}_{N_1})\boldsymbol{\phi}_1$ and $\mathrm{Tr}(\boldsymbol{\Theta}_1\mathbf{T}_1^{\mathrm{H}}) = \mathbf{t}_1^{\mathrm{H}}\boldsymbol{\phi}_1$ [38], the subproblem can be rewritten as

$$\min_{\boldsymbol{\phi}_1} \ \boldsymbol{\phi}_1^{\mathrm{H}}\boldsymbol{\Xi}_1\boldsymbol{\phi}_1 - 2\mathrm{Re}\{\mathbf{u}_1^{\mathrm{H}}\boldsymbol{\phi}_1\}, \tag{30a}$$

$$\text{s.t.}\ \ \boldsymbol{\phi}_1^{\mathrm{H}}\mathbf{P}\boldsymbol{\phi}_1 - P_1 \le 0, \tag{30b}$$

$$\boldsymbol{\phi}_1^{\mathrm{H}}\mathbf{V}\boldsymbol{\phi}_1 - P_{\boldsymbol{\phi}_1} \le 0, \tag{30c}$$

where the parameters are defined as follows

$$\boldsymbol{\Xi}_1 = |x|^2\sigma_1^2\left(\mathbf{h}_{2u}^{\mathrm{H}}\boldsymbol{\Theta}_2\mathbf{H}_{12} + \mathbf{h}_{1u}^{\mathrm{H}}\right)^{\mathrm{H}}\left(\mathbf{h}_{2u}^{\mathrm{H}}\boldsymbol{\Theta}_2\mathbf{H}_{12} + \mathbf{h}_{1u}^{\mathrm{H}}\right) \odot \mathbf{I}_{N_1} + \frac{1}{2\rho}\sum_{k=1}^{K}\left(\mathbf{b}_k\mathbf{b}_k^{\mathrm{H}} + \mathbf{L}_{1k}\right), \tag{31a}$$

$$\mathbf{P} = \mathbf{I}_{N_1} \odot \left(\mathbf{h}_{b1}\mathbf{h}_{b1}^{\mathrm{H}} + \sigma_1^2\mathbf{I}_{N_1}\right)^{\mathrm{T}}, \tag{31b}$$

$$\mathbf{u}_1 = \mathbf{t}_1 + \mathbf{f}_1 - \frac{1}{2\rho}\sum_{k=1}^{K}(\mathrm{m}_k\mathbf{b}_k + \mathbf{s}_k), \tag{31c}$$

$$\mathbf{V} = \mathbf{H}_{12}^{\mathrm{H}}\boldsymbol{\Theta}_2^{\mathrm{H}}\boldsymbol{\Theta}_2\mathbf{H}_{12} \odot \left((\mathbf{h}_{b1}\mathbf{h}_{b1}^{\mathrm{H}})^{\mathrm{T}} + \sigma_1^2\mathbf{I}_{N_1}\right), \tag{31d}$$

$$\mathbf{L}_{1k} = \sigma_1^2\left(\mathbf{d}_k^{\mathrm{H}}\mathbf{H}_{2r}\boldsymbol{\Theta}_2\mathbf{H}_{12} + \mathbf{d}_k^{\mathrm{H}}\mathbf{H}_{1r}\right)^{\mathrm{H}} \times \left(\mathbf{d}_k^{\mathrm{H}}\mathbf{H}_{2r}\boldsymbol{\Theta}_2\mathbf{H}_{12} + \mathbf{d}_k^{\mathrm{H}}\mathbf{H}_{1r}\right) \odot \mathbf{I}_{N_1}, \tag{31e}$$

$$P_{\boldsymbol{\phi}_1} = P_2 - \|\boldsymbol{\Theta}_2\mathbf{h}_{b2}\|_2^2 - \sigma_2^2\|\boldsymbol{\Theta}_2\|_2^2, \tag{31f}$$

$$\mathbf{b}_k^{\mathrm{H}} = \mathbf{d}_k^{\mathrm{H}}(\mathbf{H}_{2r}\boldsymbol{\Theta}_2\mathbf{H}_{12} + \mathbf{H}_{1r})\mathrm{diag}(\mathbf{h}_{b1}), \tag{31g}$$

$$\mathrm{m}_k = \mathbf{d}_k^{\mathrm{H}}(\mathbf{h}_{br} + \mathbf{H}_{2r}\hat{}_2\mathbf{h}_{b2}) - v_k - \rho\lambda_{k,2}. \tag{31h}$$

Because $\boldsymbol{\Xi}_1$, $\mathbf{P}$ and $\mathbf{V}$ are semidefinite matrices, subproblem (30) is convex. Thus, we can still use the Lagrange dual method to solve Problem (30). The Lagrangian function of Problem (30) is given by

$$\mathcal{L}(\boldsymbol{\phi}_1, \boldsymbol{\kappa}) = \boldsymbol{\phi}_1^{\mathrm{H}}\boldsymbol{\Xi}_1\boldsymbol{\phi}_1 - 2\mathrm{Re}\{\mathbf{u}_1^{\mathrm{H}}\boldsymbol{\phi}_1\} + \kappa_1\left(\boldsymbol{\phi}_1^{\mathrm{H}}\mathbf{P}\boldsymbol{\phi}_1 - P_1\right) + \kappa_2\left(\boldsymbol{\phi}_1^{\mathrm{H}}\mathbf{V}\boldsymbol{\phi}_1 - P_{\boldsymbol{\phi}_1}\right), \tag{32}$$

where $\boldsymbol{\kappa} = [\kappa_1, \kappa_2]^{\mathrm{T}} \succeq \mathbf{0}$ are the Lagrange multipliers associated with constraints. Then, the dual problem of (32) can be represented by

$$\max_{\boldsymbol{\kappa}} \ g(\boldsymbol{\kappa}) = \min_{\boldsymbol{\phi}_1 \in \mathcal{D}} \ \mathcal{L}(\boldsymbol{\phi}_1, \boldsymbol{\kappa}), \tag{33a}$$

$$\text{s.t.}\ \ \boldsymbol{\kappa} \succeq \mathbf{0}, \tag{33b}$$

where $\mathcal{D} = \{\boldsymbol{\phi}_1 | (30\text{b}) \cap (30\text{c})\}$ denotes the feasible domain of $\boldsymbol{\phi}_1$. Since Problem (30) is convex and satisfies the Slater condition. By setting $\partial\mathcal{L}(\boldsymbol{\phi}_1, \boldsymbol{\kappa})/\boldsymbol{\phi}_1 = 0$, the optimal solution of $\boldsymbol{\phi}_1^{\mathrm{opt}}$ is given by

$$\boldsymbol{\phi}_1^{\mathrm{opt}} = (\boldsymbol{\Xi}_1 + \kappa_1\mathbf{P} + \kappa_2\mathbf{V})^{-1}\mathbf{u}_1, \tag{34}$$

where κ_1 and κ_2 can be determined by the ellipsoid method [39].

The main idea of the ellipsoid method is to generate a series of closed sets with decreasing volumes, where each closed set contains the optimal $\boldsymbol{\kappa}$. As the number of iterations increases, the closed set will eventually converge to the optimal $\boldsymbol{\kappa}$. A common choice is to use ellipsoids of different volumes to characterize these closed sets. Therefore, the ellipsoid in the t-th iteration can be represented by

$$\Psi^{(t)} = \left\{\mathbf{z} | \left(\mathbf{z} - \boldsymbol{\kappa}^{(t)}\right)^{\mathrm{T}}\boldsymbol{\Upsilon}^{(t)}\left(\mathbf{z} - \boldsymbol{\kappa}^{(t)}\right) \le 1\right\} \tag{35}$$

Algorithm 2 Ellipsoid Method to Solve Problem (30)

1: Initial the iteration number $t = 0$, and the ellipsoid $(\boldsymbol{\Upsilon}^{(0)}, \kappa_k^{(0)})$, the accuracy ε. Let $f_{\text{obj}}(\boldsymbol{\kappa}^{(0)})$ denote the value of objective function (30a), $k \in \{1, 2\}$.
2: **repeat**
3: **if** $\boldsymbol{\kappa}^{(t)} \succeq \mathbf{0}$ **then**
4: Compute the subgradient $\mathbf{g}^{(t)}$ according to (37);
5: **else**
6: $\mathbf{g}^{(t)}(k) = \min\{\text{sgn}(\kappa_k^{(t)}), 0\}$, $k \in \{1, 2\}$;
7: **end if**
8: Normalized the subgradient $\mathbf{g}^{(t)}$ according to (36a);
9: Update $\boldsymbol{\kappa}^{(t+1)}$ according to (36b);
10: Update $\boldsymbol{\Upsilon}^{(t+1)}$ according to (36c);
11: $t = t + 1$;
12: Calculate the value of f_{obj};
13: **until** $\frac{\left|f_{\text{obj}}(\boldsymbol{\kappa}^{(t+1)}) - f_{\text{obj}}(\boldsymbol{\kappa}^{(t)})\right|}{f_{\text{obj}}(\boldsymbol{\kappa}^{(t)})} \leq \varepsilon$.

where $\boldsymbol{\kappa}$ and $\boldsymbol{\Upsilon}^{(t)} \in \mathbb{S}_{++}^n$ denote the center of $\Psi^{(t)}$ and the size and shape of $\Psi^{(t)}$, respectively. According to [39], the update criteria are given as follows:

$$\tilde{\mathbf{g}}^{(t)} = \frac{1}{\sqrt{\left(\mathbf{g}^{(t)}\right)^{\mathrm{T}} \boldsymbol{\Upsilon} \mathbf{g}^{(t)}}} \mathbf{g}^{(t)}, \tag{36a}$$

$$\boldsymbol{\kappa}^{(t+1)} = \boldsymbol{\kappa}^{(t)} - \frac{1}{n+1} \boldsymbol{\Upsilon}^{(t)} \tilde{\mathbf{g}}^{(t)}, \tag{36b}$$

$$\boldsymbol{\Upsilon}^{(t+1)} = \frac{n^2}{n^2 - 1} \left(\boldsymbol{\Upsilon}^{(t)} - \frac{2}{(n+1)} \boldsymbol{\Upsilon}^{(t)} \tilde{g}^{(t)} (\tilde{g}^{(t)})^{\mathrm{T}} \boldsymbol{\Upsilon}^{(t)} \right), \tag{36c}$$

where $\mathbf{g}^{(t)}$ denotes the subgradient. For Problem (33), the subgradient is calculated as

$$\mathbf{g}^{(t)} = \begin{bmatrix} \boldsymbol{\phi}_1^{\mathrm{H}} \mathbf{P} \boldsymbol{\phi}_1 - P_1 \\ \boldsymbol{\phi}_1^{\mathrm{H}} \mathbf{V} \boldsymbol{\phi}_1 - P_{\boldsymbol{\phi}_1} \end{bmatrix}. \tag{37}$$

Furthermore, if $\boldsymbol{\kappa}$ is not feasible, i.e., $\exists\ \kappa_k < 0, k \in \{1, 2\}$, the corresponding subgradient can be calculated as $\mathbf{g}^{(t)}(k) = \min\{\text{sgn}(\kappa_k^{(t)}), 0\}$, $k \in \{1, 2\}$. Based on the above analysis, the overall algorithm is summarized in Algorithm 2.

5) Optimizing the Phase Shift $\boldsymbol{\Theta}_2$: We optimize $\boldsymbol{\Theta}_2$ while fixing the other variables. Firstly, we define $\mathbf{T}_2 \triangleq x^* \sqrt{P_{\text{t}}^{\text{act}}} \mathbf{h}_{2u} \mathbf{h}_{b1}^{\mathrm{H}} \boldsymbol{\Theta}_1^{\mathrm{H}} \mathbf{H}_{12}^{\mathrm{H}}$, $\mathbf{F}_2 \triangleq x^* \sqrt{P_{\text{t}}^{\text{act}}} \mathbf{h}_{2u} \mathbf{h}_{b2}^{\mathrm{H}}$, $\mathbf{M}_1 \triangleq \sigma_1^2 |x|^2 \mathbf{h}_{2u} \mathbf{h}_{1u}^{\mathrm{H}} \boldsymbol{\Theta}_1 \boldsymbol{\Theta}_1^{\mathrm{H}} \mathbf{H}_{12}^{\mathrm{H}}$, $\mathbf{M}_{2k} \triangleq \mathbf{H}_{2r}^{\mathrm{H}} \mathbf{d}_k \mathbf{d}_k^{\mathrm{H}} \mathbf{H}_{1r} \boldsymbol{\Theta}_1 \boldsymbol{\Theta}_1^{\mathrm{H}} \mathbf{H}_{12}^{\mathrm{H}}$, $\mathbf{G}_k \triangleq \mathbf{H}_{2r}^{\mathrm{H}} \mathbf{d}_k (\mathbf{t}_k + \rho \boldsymbol{\lambda}_{k,\text{t}})^{\mathrm{H}}$, and $\mathbf{Q}_k \triangleq \mathbf{H}_{2r}^{\mathrm{H}} \mathbf{d}_k (\mathbf{e}_k + \rho \boldsymbol{\lambda}_{k,\text{e}})^{\mathrm{H}} \mathbf{H}_{12}^{\mathrm{H}} \boldsymbol{\Theta}_1^{\mathrm{H}}$. $\mathbf{t}_2$, $\mathbf{f}_2$, $\mathbf{m}_1$, $\mathbf{m}_{2k}$, $\mathbf{g}_k$, and $\mathbf{q}_k$ are the collection of diagonal elements of matrix $\mathbf{T}_2$, $\mathbf{F}_2$, $\mathbf{M}_1$, $\mathbf{M}_{2k}$, $\mathbf{G}_k$, and $\mathbf{Q}_k$, respectively.

Then, by using the similar method used to optimize $\boldsymbol{\Theta}_1$, this subproblem can be formulated as

$$\min_{\boldsymbol{\phi}_2} \quad \boldsymbol{\phi}_2^{\mathrm{H}} \boldsymbol{\Xi}_2 \boldsymbol{\phi}_2 - 2\text{Re}\{\mathbf{u}_2^{\mathrm{H}} \boldsymbol{\phi}_2\} \tag{38a}$$

$$\text{s.t.} \quad \boldsymbol{\phi}_2^{\mathrm{H}} \mathbf{Z} \boldsymbol{\phi}_2 \leq P_2, \tag{38b}$$

where the parameters are defined as follows

$$\boldsymbol{\Xi}_2 = |x|^2 \mathbf{h}_{2u} \mathbf{h}_{2u}^{\mathrm{H}} \odot \left(\sigma_1^2 (\mathbf{H}_{12} \boldsymbol{\Theta}_1 \boldsymbol{\Theta}_1^{\mathrm{H}} \mathbf{H}_{12}^{\mathrm{H}})^{\mathrm{T}} + \sigma_2^2 \mathbf{I}_{N_2} \right) + \frac{1}{2\rho} \left(\sum_{k=1}^{K} \mathbf{r}_k \mathbf{r}_k^{\mathrm{H}} + \mathbf{L}_{2k} \right), \tag{39a}$$

$$\mathbf{Z} = \mathbf{I}_{N_2} \odot ((\mathbf{H}_{12} \boldsymbol{\Theta}_1 \mathbf{h}_{b1} \mathbf{h}_{b1}^{\mathrm{H}} \boldsymbol{\Theta}_1^{\mathrm{H}} \mathbf{H}_{12}^{\mathrm{H}})^{\mathrm{T}} + (\mathbf{h}_{b2} \mathbf{h}_{b2}^{\mathrm{H}} + \sigma_2^2 \mathbf{I}_{N_2})^{\mathrm{T}} + \sigma_1^2 (\mathbf{H}_{12} \boldsymbol{\Theta}_1 \boldsymbol{\Theta}_1^{\mathrm{H}} \mathbf{H}_{12}^{\mathrm{H}})^{\mathrm{T}}), \tag{39b}$$

$$\mathbf{L}_{2k} = \left(\mathbf{H}_{2r}^{\mathrm{H}} \mathbf{d}_k \mathbf{d}_k^{\mathrm{H}} \mathbf{H}_{2r} \right) \odot \left((\mathbf{H}_{12} \boldsymbol{\Theta}_1 \boldsymbol{\Theta}_1^{\mathrm{H}} \mathbf{H}_{12}^{\mathrm{H}})^{\mathrm{T}} + \mathbf{I}_{N_2} \right), \tag{39c}$$

$$\mathbf{u}_2 = \mathbf{t}_2 + \mathbf{f}_2 + \mathbf{m}_1 - \frac{1}{2\rho} \sum_{k=1}^{K} (\text{n}_k \mathbf{r}_k + \mathbf{m}_{2k} + \mathbf{g}_k + \mathbf{q}_k), \tag{39d}$$

$$\mathbf{r}_k^{\mathrm{H}} = \mathbf{d}_k^{\mathrm{H}} \mathbf{H}_{2r} (\text{diag}(\mathbf{H}_{12} \boldsymbol{\Theta}_1 \mathbf{h}_{b1}) + \text{diag}(\mathbf{h}_{b2})), \tag{39e}$$

$$\text{n}_k = \mathbf{d}_k^{\mathrm{H}} (\mathbf{h}_{br} + \mathbf{H}_{1r} \boldsymbol{\Theta}_1 \mathbf{h}_{b1}) - v_k - \rho \lambda_{k,2}. \tag{39f}$$

Then, we can get the optimal solution of $\boldsymbol{\phi}_2^{\text{opt}}$, given by

$$\boldsymbol{\phi}_2^{\text{opt}} = (\boldsymbol{\Xi}_2 + \xi \mathbf{Z})^{-1} \mathbf{u}_2, \tag{40}$$

where $\xi \geq 0$ is the Lagrange multiplier associated with constraints which can be determined by the bisection search method.

D. The Overall Algorithm for Solving the Optimization Problem

As shown in Algorithm 3, there are two loops in the PDD framework. For the inner loop of the PDD framework, we use the BCD method to divide the original problem into several subproblems. Then, we solve the subproblems using the Lagrange dual method with the bisection search method and the ellipsoid method. For the outer loop, we update the dual variables and penalty factors according to the value of constraint violation.

The computational complexity of the proposed PDD-based algorithm can be represented by

$$\mathcal{O}(I_{\text{outer}} I_{\text{inner}} (o_1 + o_2 + o_3 + o_4 + o_5)), \tag{41}$$

where $o_1 = (M^3 + M^2 + (K^3 M^3 + K^2 M^2) log \frac{I_0}{\varepsilon})$, $o_2 = K(M^2(N_1 + N_2) + log \frac{I_0}{\varepsilon}(M^3 + M^2))$, $o_3 = Klog \frac{I_0}{\varepsilon}(M^2 + MN_1 + MN_2)$, $o_4 = (N_1 N_2 + MN_2 + MN_1 + N_1^2 + N_2^2 + (N_1^3 + N_1^2) log \frac{RG}{\varepsilon})$, and $o_5 = (M^2 N_2 + N_1^2 N_2 + N_1 N_2^2 + (N_2^3 + N_2^2) log \frac{I_0}{\varepsilon})$ denote the computational complexity of optimizing $\{\mathbf{w}_k\}$, $\{\mathbf{d}_k\}$, $\{u_k, v_k, y_k, \mathbf{e}_k, \mathbf{t}_k\}$, $\boldsymbol{\Theta}_1$, and $\boldsymbol{\Theta}_2$, respectively. I_{outer} and I_{inner} denote the number of outer loop iterations and inner loop iterations, respectively. I_0 is the initial interval of the bisection-search method. G and R denote maximum length of the sub-gradients and the length of the semi-axes on the initial ellipsoid.

It can be observed that the computational complexity of the proposed algorithm is mainly dominated by $\mathcal{O}(I_{\text{outer}} I_{\text{inner}} (M^3 + N_1^3 + N_2^3))$, which is acceptable in the analysis of beamforming design [15], [22]. Besides, due to the application of Lagrangian dual method and ellipsoid method, the computational complexity of our proposed algorithm has been much lower than compared to the interior point.

Algorithm 3 Low-Complexity Algorithm Based on PDD Framework

Initial the iteration number $t=0$, the tolerance of accuracy ε, $\rho^{(0)}>0$, $\sigma>0$, $0<c<1$, feasible $\mathbf{\Omega}_1^{(0)}$. Calculate the objective function value of Problem (20), denoted as $\mathcal{P}(\mathbf{\Omega}_1^{(0)},\rho^{(0)},\boldsymbol{\lambda}^{(0)})$, and the achievable data rate in (6), denoted as $R^{(0)}$. $\boldsymbol{\lambda}^{(0)}$ is the collection of dual parameters $\{\lambda_{k,2}^{(0)},\lambda_{k,3}^{(0)},\boldsymbol{\lambda}_{k,\mathrm{e}}^{\mathrm{T}(0)},\boldsymbol{\lambda}_{k,\mathrm{t}}^{\mathrm{T}(0)}\}$. $h^{(0)}=\max\{|u_k-\mathbf{d}_k^{\mathrm{H}}\mathbf{A}_k\mathbf{w}_k|,|v_k-\mathbf{d}_k^{\mathrm{H}}\mathbf{q}|,|y_k-\sum_{m=1,m\neq k}^{K}\mathbf{d}_k^{\mathrm{H}}\mathbf{A}_m\mathbf{w}_k|,|\mathbf{e}_k^{\mathrm{H}}-\mathbf{d}_k^{\mathrm{H}}\mathbf{B}|,|\mathbf{t}_k^{\mathrm{H}}-\mathbf{d}_k^{\mathrm{H}}\mathbf{C}|\}$ denote the maximum value of constraint violation between (13a), (13b), (13c), (13d) and (13e).
repeat
  repeat
    By fixing the other variables, calculate the optimal value of $\mathbf{w}_k^{(t+1)}$ in (23);
    By fixing the other variables, calculate the optimal value of $\mathbf{d}_k^{(t+1)}$ in (26);
    By fixing the other variable, alternately calculate the optimal value of $\{x^{(t+1)},u_k^{(t+1)},v_k^{(t+1)},y_k^{(t+1)},\mathbf{e}_k^{(t+1)},\mathbf{t}_k^{(t+1)}\}$ in (28) and (29), respectively;
    By fixing the other variable, alternately calculate the optimal value of $\mathbf{\Theta}_1^{(t+1)}$, $\mathbf{\Theta}_2^{(t+1)}$ in (34) and (40), respectively;
    Calculate the objective function value: $\mathcal{P}(\mathbf{\Omega}_1^{(t+1)},\rho^{(t+1)},\boldsymbol{\lambda}^{t+1})$;
  until $\frac{\left|\mathcal{P}(\mathbf{\Omega}_1^{(t+1)},\rho^{(t+1)},\boldsymbol{\lambda}^{(t+1)})-\mathcal{P}(\mathbf{\Omega}_1^{(t)},\rho^{(t)},\boldsymbol{\lambda}^{(t)})\right|}{\mathcal{P}(\mathbf{\Omega}_1^{(t)},\rho^{(t)},\boldsymbol{\lambda}^{(t)})}\leq\varepsilon$
  Compute the maximum value of constraint violation $h^{(t+1)}$;
  Compute the achievable data rate $R^{(t+1)}$;
  if $h^{(t+1)}\leq\sigma$ **then**
    $\boldsymbol{\lambda}^{(t+1)}=\boldsymbol{\lambda}^{(t)}+\frac{1}{\rho^{(t)}}\mathbf{h}^{(t+1)}$, $\rho^{(t+1)}=\rho^{(t)}$;
  else
    $\boldsymbol{\lambda}^{(t+1)}=\boldsymbol{\lambda}^{(t)}$, $\rho^{(t+1)}=c\rho^{(t)}$;
  end if
  $t=t+1$;
until $\frac{|R^{(t+1)}-R^{(t)}|}{R^{(t)}}\leq\varepsilon$

IV. Joint Beamforming Design Algorithm for Passive RIS

In this section, we consider the double passive RIS-assisted RCC system to provide a comparison benchmark scheme for double active RIS-assisted RCC systems. Unlike active RIS, passive RIS does not amplify the thermal noise, at the cost of severe signal attenuation. In addition, for each element in the phase shift matrix of the passive RIS, we have unit-modulus constraints, i.e., $|\boldsymbol{\phi}_1(n)|=1,n=1,\ldots,N_1$, $|\boldsymbol{\phi}_2(n)|=1$, $n=1,\ldots,N_2$. Therefore, the original Problem (20) for double passive RISs can be formulated as

$$\begin{aligned}\min_{\mathbf{\Omega}_2}\ & -\frac{P_{\mathrm{t}}^{\mathrm{pas}}}{\sigma_0^2}|h_{\mathrm{bu}}+\mathbf{h}_{2u}^{\mathrm{H}}\mathbf{\Theta}_2\mathbf{H}_{12}\mathbf{\Theta}_1\mathbf{h}_{b1}+\mathbf{h}_{1u}^{\mathrm{H}}\mathbf{\Theta}_1\mathbf{h}_{b1}\\ &+\mathbf{h}_{2u}^{\mathrm{H}}\mathbf{\Theta}_2\mathbf{h}_{b2}|^2\\ &+\frac{1}{2\rho}\sum_{k=1}^{K}\left|u_k-\mathbf{d}_k^{\mathrm{H}}\mathbf{A}_k\mathbf{w}_k+\rho\lambda_{k,1}\right|^2\\ &+\frac{1}{2\rho}\sum_{k=1}^{K}\left|v_k-\mathbf{d}_k^{\mathrm{H}}\mathbf{q}+\rho\lambda_{k,2}\right|^2\\ &+\frac{1}{2\rho}\left|y_{k,m}-\mathbf{d}_k^{\mathrm{H}}\mathbf{A}_m\mathbf{w}_k+\rho\lambda_{k,3}\right|^2, &(42a)\\ \text{s.t.}\ & \eta\left(|y_k|^2+P_{\mathrm{t}}^{\mathrm{pas}}|v_k|^2+\sigma^2\left\|\mathbf{d}_k^{\mathrm{H}}\right\|_2^2\right)\\ &-2\mathrm{Re}\left((u_k^{(i)})^*u_k\right)+\left|u_k^{(i)}\right|^2\leq 0, &(42b)\\ &\sum_{k=1}^{K}\|\mathbf{w}_k\|^2\leq P_{\mathrm{r}}, &(42c)\\ &|\boldsymbol{\phi}_1(n)|=1,n=1,\ldots,N_1, &(42d)\\ &|\boldsymbol{\phi}_2(n)|=1,n=1,\ldots,N_2, &(42e)\end{aligned}$$

where $\mathbf{\Omega}_2=\{\mathbf{w}_k,\mathbf{d}_k,\mathbf{\Theta}_1,\mathbf{\Theta}_2,u_k,v_k,y_k\}$, $P_{\mathrm{t}}^{\mathrm{pas}}$ denote the transmitted power at BS. Since this problem is similar to Problem (20), we can still use the BCD algorithm to optimize each variable separately. The optimal solutions of $\{\mathbf{w}_k,\mathbf{d}_k,u_k,v_k,y_k\}$ for passive RIS have the same form as in the active RIS scenario. Therefore, in the following part, we just discuss how to design the phase shift variable $\mathbf{\Theta}_1$ and $\mathbf{\Theta}_2$ for passive RISs.

1) Optimizing Phase Shift $\mathbf{\Theta}_1$: The original Problem (42) can be rewritten as

$$\begin{aligned}\max_{\boldsymbol{\phi}_1}\ & \boldsymbol{\phi}_1^{\mathrm{H}}\mathbf{\Xi}_3\boldsymbol{\phi}_1-2\mathrm{Re}\{\boldsymbol{\phi}_1^{\mathrm{H}}\mathbf{s}_1\}, &(43a)\\ \text{s.t.}\ & |\boldsymbol{\phi}_1(m)|=1,m=1,\ldots,N_1, &(43b)\end{aligned}$$

where the parameters are defined as follows

$$\begin{aligned}&\mathbf{\Xi}_3=\mathbf{a}\mathbf{a}^{\mathrm{H}}-\frac{1}{2\rho}\sum_{k=1}^{K}\mathbf{b}_k\mathbf{b}_k^{\mathrm{H}},\mathbf{s}_1=\frac{1}{2\rho}\sum_{k=1}^{K}\mathbf{b}_k\mathrm{m}_k-a_0\mathbf{a}, &(44a)\\ &a_0=h_{bu}+\mathbf{h}_{2u}^{\mathrm{H}}\mathbf{\Theta}_2\mathbf{h}_{b2}, &(44b)\\ &\mathbf{a}^{\mathrm{H}}=\left(\mathbf{h}_{2u}^{\mathrm{H}}\mathbf{\Theta}_2\mathbf{H}_{12}+\mathbf{h}_{1u}^{\mathrm{H}}\right)\mathrm{diag}(\mathbf{h}_{b1}). &(44c)\end{aligned}$$

Since Problem (43) has unit-modulus constraints, it is a non-convex problem. We can use the MM algorithm to solve this problem [40].

For any given solution $\boldsymbol{\phi}_1^t$ at the t-th iteration and for any feasible $\boldsymbol{\phi}_1$, we have

$$\begin{aligned}\boldsymbol{\phi}_1^{\mathrm{H}}\mathbf{\Xi}_3\boldsymbol{\phi}_1\geq\ & 2\mathrm{Re}\left\{\boldsymbol{\phi}_1^{\mathrm{H}}(\mathbf{\Xi}_3-\lambda_{\min}\mathbf{I}_{N1})\boldsymbol{\phi}_1^t\right\}\\ &+(\boldsymbol{\phi}_1^t)^{\mathrm{H}}(\lambda_{\min}\mathbf{I}_{N1}-\mathbf{\Xi}_3)\boldsymbol{\phi}_1^t+\lambda_{\min}N_1, &(45)\end{aligned}$$

where $\lambda_{\min}$ is the minimum eigenvalue of $\mathbf{\Xi}_3$.

Thus, Problem (43) can be transformed into a more tractable form as follows

$$\begin{aligned}\max_{\boldsymbol{\phi}_1}\ & 2\mathrm{Re}\left\{\boldsymbol{\phi}_1^{\mathrm{H}}\mathbf{v}_1^t\right\}, &(46a)\\ \text{s.t.}\ & |\boldsymbol{\phi}_1(n)|=1,n=1,\ldots,N_1, &(46b)\end{aligned}$$

where $\mathbf{v}_1^t=(\mathbf{\Xi}_3-\lambda_{\min}\mathbf{I}_{N_1})\boldsymbol{\phi}_1^t-\mathbf{s}_1$.

Then, the optimal solution $\boldsymbol{\phi}_1^{\mathrm{opt}}$ can be given by

$$\boldsymbol{\phi}_1^{(t+1)}=e^{j\angle(\mathbf{v}_1^t)}. \quad (47)$$

Algorithm 4 MM Method to Solve Problem (43)

1: Initialize $t = 0$, $\boldsymbol{\phi}_1^{(t)}$;
2: **repeat**
3: Compute the value of $\mathbf{v}_1^t$;
4: Update $\boldsymbol{\phi}_1^{(t+1)} = e^{j\angle(\mathbf{v}_1^t)}$;
5: **until** the objective function converges.

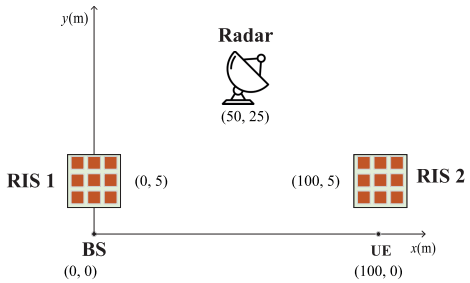

Fig. 2. Simulation proposition.

The overall algorithm to solve Problem (46) is summarized in Algorithm 4.

2) Optimizing Phase Shift $\boldsymbol{\Theta}_2$: For this subproblem, we can still optimize the phase shift matrix $\boldsymbol{\Theta}_2$ by using the same method as optimizing the matrix $\boldsymbol{\Theta}_1$. Therefore, the original Problem (42) can be transformed into

$$\max_{\boldsymbol{\phi}_2} \quad 2\mathrm{Re}\left\{\boldsymbol{\phi}_2^{\mathrm{H}}\mathbf{v}_2^t\right\}, \tag{48a}$$

$$\text{s.t.} \quad |\boldsymbol{\phi}_2(n)| = 1, n = 1, \ldots, N_2, \tag{48b}$$

where the parameters can be defined as follows

$$\mathbf{v}_2^t = \left(\boldsymbol{\Xi}_4 - \lambda_{\min}\mathbf{I}_{N_2}\right)\boldsymbol{\phi}_2^t - \sum_{k=1}^{K}\frac{1}{2\rho}\mathbf{r}_k \mathrm{n}_k + b_0\mathbf{b}, \tag{49a}$$

$$\boldsymbol{\Xi}_4 = \mathbf{b}\mathbf{b}^{\mathrm{H}} - \frac{1}{2\rho}\sum_{k=1}^{K}\mathbf{R}_k, b_0 = h_{bu} + \mathbf{h}_{1u}^{\mathrm{H}}\boldsymbol{\Theta}_1\mathbf{h}_{b1}, \tag{49b}$$

$$\mathbf{b}^{\mathrm{H}} = \mathbf{h}_{2u}^{\mathrm{H}}(\mathrm{diag}(\mathbf{H}_{12}\boldsymbol{\Theta}_1\mathbf{h}_{b1}) + \mathrm{diag}(\mathbf{h}_{b2})). \tag{49c}$$

Finally, the optimal solution $\boldsymbol{\phi}_2^{\mathrm{opt}}$ can be given by

$$\boldsymbol{\phi}_2^{(t+1)} = e^{j\angle(\mathbf{v}_2^t)}. \tag{50}$$

V. Simulation Results

In this section, numerical results are provided to demonstrate the advantages of using double active RISs compared with single active RIS and double passive RISs in RCC systems.

A. Simulation Parameter Setting

As shown in Fig. 2, we consider a double RIS-assisted RCC system with two-dimensional coordinates where the location of BS, UE, active RIS 1, active RIS 2, and radar are set to (0 m, 0 m), (100 m, 0 m), (0 m, 5 m), (100 m, 5 m), and (50 m, 25 m), respectively. Both BS and UE are equipped with a single antenna. According to [15], [22], the default setting of radar-related parameters are specified in the "Radar Model" block of Table I.

The large-scale path loss of the channel in dB is modelled as

$$\mathrm{PL} = \mathrm{PL}_0 - 10\alpha\log_{10}\left(\frac{d}{d_0}\right), \tag{51}$$

where α is the large-scale path-loss factor, PL_0 is the path-loss value when the reference distance is d_0, and d is the distance between the transmitter and the receiver. In our simulations, we assume $d_0 = 1$ m, and $\mathrm{PL}_0 = -30$ dB. The path loss factors for channel h_{bu}, $\mathbf{h}_{b1}$, $\mathbf{h}_{2u}^{\mathrm{H}}$, $\mathbf{h}_{b2}$, $\mathbf{h}_{1u}^{\mathrm{H}}$, $\mathbf{h}_{br}$, $\mathbf{H}_{1r}$, $\mathbf{H}_{2r}$, and $\mathbf{H}_{12}$ are denoted by $\alpha_{\mathrm{BS-UE}}$, $\alpha_{\mathrm{BS-RIS1}}$, $\alpha_{\mathrm{RIS2-UE}}$, $\alpha_{\mathrm{BS-RIS2}}$, $\alpha_{\mathrm{RIS1-UE}}$, $\alpha_{\mathrm{BS-Radar}}$, $\alpha_{\mathrm{RIS1\text{-}Radar}}$, $\alpha_{\mathrm{RIS2-Radar}}$ and $\alpha_{\mathrm{RIS1\text{-}RIS2}}$, respectively. The long distance between the BS and UE increases the likelihood of encountering additional obstacles and scatterers. Consequently, the path loss factor for this link is assumed to be 3.75. Moreover, the double reflection link (RIS 1-RIS 2) has the capability to circumvent obstacles more effectively thanks to their deployment locations, increasing the likelihood of establishing a communication link with low path loss [41]. Therefore, the default setting of path loss factors are specified in the "Communication Model" block of Table I.

The small-scale fading which follows Rician fading can be modeled as

$$\tilde{\mathbf{H}} = \sqrt{\frac{\beta}{\beta+1}}\tilde{\mathbf{H}}^{\mathrm{LoS}} + \sqrt{\frac{1}{\beta+1}}\tilde{\mathbf{H}}^{\mathrm{NLoS}}, \tag{52}$$

where β is the factor of Rician fading. $\tilde{\mathbf{H}}^{\mathrm{LoS}}$ and $\tilde{\mathbf{H}}^{\mathrm{NLoS}}$ respectively denote the line of sight (LoS) and the non-LoS (NLoS) channel which follows Rayleigh fading. $\tilde{\mathbf{H}}^{\mathrm{LoS}}$ can be modeled as $\tilde{\mathbf{H}}^{\mathrm{LoS}} = \mathbf{a}_{D_r}(\vartheta^{AoA})\mathbf{a}_{D_t}^{\mathrm{H}}(\vartheta^{AoD})$, where

$$\mathbf{a}_{D_r}\left(\vartheta^{AoA}\right) = \left[1, e^{j\frac{2\pi d}{\lambda}\sin\vartheta^{AoA}}, \ldots, e^{j\frac{2\pi d}{\lambda}(D_r-1)\sin\vartheta^{AoA}}\right]^{\mathrm{T}}, \tag{53}$$

and

$$\mathbf{a}_{D_t}\left(\vartheta^{AoD}\right) = \left[1, e^{j\frac{2\pi d}{\lambda}\sin\vartheta^{AoD}}, \ldots, e^{j\frac{2\pi d}{\lambda}(D_t-1)\sin\vartheta^{AoD}}\right]^{\mathrm{T}}, \tag{54}$$

where λ, d, ϑ^{AoA}, and ϑ^{AoD} represent the wavelength, the separating distance of antennas, the arrival angle, and departure angle, respectively. Both ϑ^{AoA} and ϑ^{AoD} follow a random distribution within $[0, 2\pi]$. D_t and D_r denote the number of antennas/reflecting elements of RIS in the transmitter and the receiver, respectively. The default setting of other parameters are specified in Table I.

B. Benchmark Schemes

To verify the advantages of deploying double active RISs in the RCC system, we compare the performance between the following schemes:

- *Double active RISs (DAR):* Two active RISs are deployed in the RCC system. The corresponding algorithm in this scheme is based on Algorithm 3.
- *Double passive RISs (DPR):* Two passive RISs are deployed in the RCC system. The corresponding algorithm in this scheme is based on Section IV.

TABLE I
SIMULATION CONFIGURATIONS

Description	Parameter and Value
Radar model	$M = 12$, $K = 7$, $\theta_k \in [-\pi/2, -\pi/3, -\pi/6, 0, \pi/6, \pi/3, \pi/2]$, $\alpha_k = 10^{-1}, \forall k \in \mathcal{K}$, $\eta = 20$ dB.
Communication model	$N_1 = N_2 = 40$, $d/\lambda = 1/2$, $\beta = 3$, $\alpha_{\text{BS-UE}} = 3.75$, $\alpha_{\text{BS-RIS1}} = \alpha_{\text{RIS2-UE}} = 2.5$, $\alpha_{\text{BS-RIS2}} = \alpha_{\text{RIS1-UE}} = 3$, and $\alpha_{\text{BS-Radar}} = \alpha_{\text{RIS1-Radar}} = \alpha_{\text{RIS2-Radar}} = \alpha_{\text{RIS1-RIS2}} = 2.2$, $\sigma^2 = {\sigma_0}^2 = {\sigma_1}^2 = {\sigma_2}^2 = -80$ dBm
Power model	$P_{\text{SW}} = -10$ dBm, $P_{\text{DC}} = -5$ dBm, $Q_{\text{total}} = 11$ W, $\gamma = 0.9$
Others	$\varepsilon = 10^{-3}$.

- *Single active RIS i (SAR):* Single active RIS i is deployed in the RCC system. For the case of deploying single active RIS 1 near the BS, we set $\mathbf{H}_{12} = \mathbf{0}$, $\mathbf{H}_{2r} = \mathbf{0}$, $\mathbf{h}_{b2} = \mathbf{0}$, $\mathbf{h}_{2u}^{\text{H}} = \mathbf{0}$, and skip the step of optimizing $\mathbf{\Theta}_2$ in the proposed algorithm. For the case of deploying single active RIS 2 near the UE, we set $\mathbf{H}_{12} = \mathbf{0}$, $\mathbf{H}_{1r} = \mathbf{0}$, $\mathbf{h}_{b1} = \mathbf{0}$, $\mathbf{h}_{1u}^{\text{H}} = \mathbf{0}$, and skip the step of optimizing $\mathbf{\Theta}_1$ in the proposed algorithm.
- *No RIS (NR):* RIS is not deployed in the RCC system. Specifically, we set $\mathbf{H}_{1r} = \mathbf{0}$, $\mathbf{H}_{2r} = \mathbf{0}$, $\mathbf{H}_{12} = \mathbf{0}$, $\mathbf{h}_{2u}^{\text{H}} = \mathbf{0}$, and $\mathbf{h}_{1u}^{\text{H}} = \mathbf{0}$. Then, we skip the steps for optimizing $\mathbf{\Theta}_1$ and $\mathbf{\Theta}_2$ in the proposed algorithm.

Then, based on the power model in [21], the total power consumption models for the above schemes are described respectively as follows

$$Q_{\text{total}}^{\text{DAR}} = P_{\text{t}}^{\text{act}} + P_{\text{r}} + P_1 + P_2 + (N_1 + N_2)(P_{\text{SW}} + P_{\text{DC}}), \tag{55a}$$
$$Q_{\text{total}}^{\text{DPR}} = P_{\text{t}}^{\text{pas}} + P_{\text{r}} + (N_1 + N_2)P_{\text{SW}}, \tag{55b}$$
$$Q_{\text{total}}^{\text{SAR}} = P_{\text{t}}^{\text{act}} + P_i + P_{\text{r}} + N_i(P_{\text{SW}} + P_{\text{DC}}), \forall i \in \{1, 2\}, \tag{55c, 55d}$$
$$Q_{\text{total}}^{\text{NR}} = P_{\text{t}}^{\text{no}} + P_{\text{r}}, \tag{55e}$$

where P_{SW} and P_{DC} denote the power consumption of the switch and control circuit for each RIS reflecting element, the direct current bias power for each active reflecting element, respectively.

In the following simulations, we compare the performance difference between the above schemes with the same total power budget and the same total number of reflecting elements of RISs for fairness. Thus, we define the total system power budget as $Q_{\text{total}} = Q_{\text{total}}^{\text{DAR}} = Q_{\text{total}}^{\text{DAR}} = Q_{\text{total}}^{\text{SAR}} = Q_{\text{total}}^{\text{NR}}$. Then, the relationship between the radar power budget and the total system power budget is given by

$$P_{\text{r}} = \gamma Q_{\text{total}}, \tag{56}$$

where $\gamma \in [0, 1]$ represents the power allocation factor. Unless specified otherwise, we set $P_{\text{t}}^{\text{act}} = P_1 = P_2$. The default setting of the above power model related parameters are listed in the Table I.

C. Convergence Behavior of the Proposed Algorithm

In this subsection, we set $P_{\text{r}} = 10$ W, $P_{\text{t}}^{\text{act}} = P_1 = P_2 = 0.4$W. Fig. 3 illustrates the convergence behavior of the proposed algorithm. It is shown that the algorithm quickly converges within about 10 iterations and the value of the constraint violation reaches the level of 10^{-6}, which allows the equation constraint to hold and ensure the feasibility of the PDD algorithm.

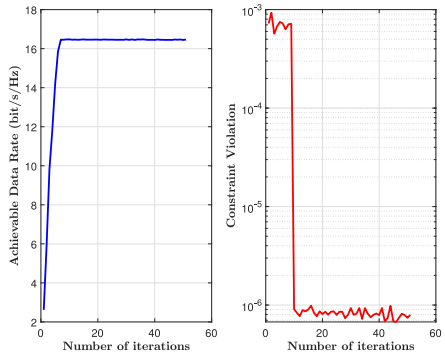

Fig. 3. Convergence behavior of PDD algorithm.

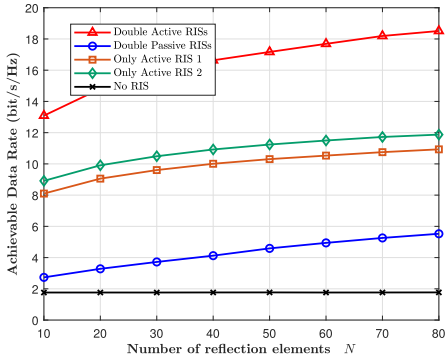

Fig. 4. Achievable data rate versus the total number of reflecting elements.

D. The Impact of the Number of Reflecting Elements

Fig. 4 shows the achievable data rate versus the number of reflecting elements. Note that the total number of elements $N = N_1 + N_2$ is the same for different schemes. As shown in Fig. 4, the achievable data rate of the double active RIS-assisted system significantly outperforms the other benchmarks. It illustrates that active RIS can effectively overcome the "multiplicative fading" effect introduced by passive RIS. Furthermore, the double active RIS-assisted RCC system performs better than the single active RIS-assisted RCC system. This illustrates that deploying double active RISs in RCC system can yield cooperative benefits, thereby enhancing the achievable data rate.

E. The Impact of the Location of RIS

In Fig. 5, we investigate the impact of the locations of two RISs on the achievable data rate by moving the positions of two RISs. By denoting the horizontal coordinate of the RIS 1 as x, the locations of RIS 1 and RIS 2 are set to (x m, 0 m), ($100 - x$ m, 0 m), respectively. It can be seen that the double active RIS-assisted system achieves superior performance over other schemes in all locations. It is interesting to observe that,

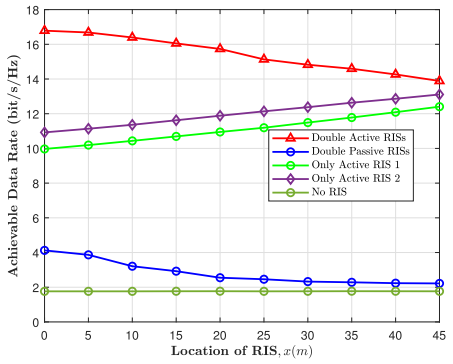

Fig. 5. Achievable data rate versus locations of RIS, $x(m)$.

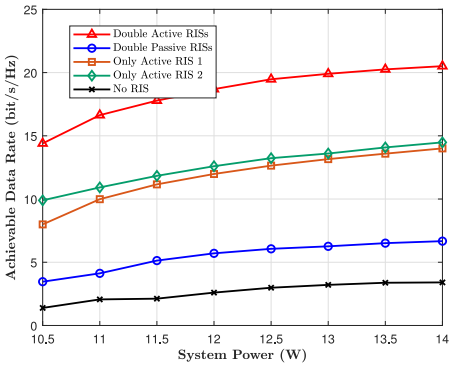

Fig. 6. Achievable data rate versus total system power.

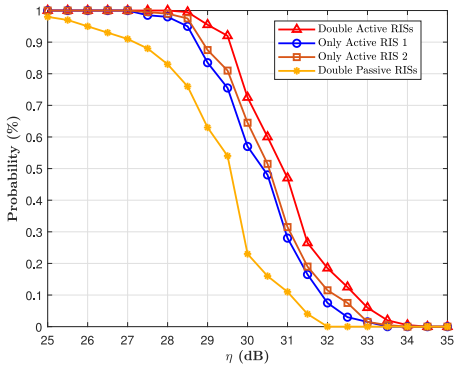

Fig. 7. Successful probability of a feasible solution versus η.

as x increases, the achievable data rate of the double active RIS-assisted system decreases while data rate of the single active RIS-assisted system increases. This is because as x increase, the power of the signal received by UE decreases due to the increased path loss of the RIS 2-UE link and BS-RIS 1 link. Furthermore, the achievable data rate of the two schemes reaches the same level at about $x = 45$ m. It shows that the double RISs can be regarded as a single RIS equipped with $N_1 + N_2$ reflecting elements as the two RISs get closer to each other.

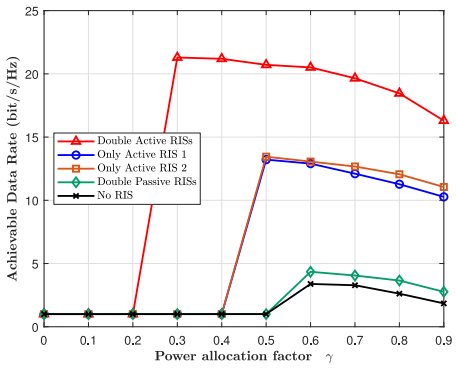

Fig. 8. Achievable data rate versus γ.

F. The Impact of the Total System Power

In Fig. 6, we compare the achievable data rate versus the total system power budget. It can be seen that the double active RIS-assisted RCC system exhibits better system performance than the other benchmarks, as the total system power budget increases. Thus, deploying double active RISs in RCC systems can effectively reduce system power consumption while guaranteeing the required achievable data rate.

G. The Successful Probability of a Feasible Solution Versus η

In Fig. 7, we study the successful probability of a feasible solution versus radar SINR requirements, i.e., η. As η increases, it becomes more difficult to find a feasible solution that satisfies radar SINR requirements. When $\eta = 29$ dB, the double active RIS-assisted RCC system exhibits a probability of over 95% to find a feasible solution, whereas the double passive RIS-assisted RCC system has only about a 60% probability of finding a feasible solution. This clearly shows that interference between the radar and the communication system limits the improvement of radar detection performance, i.e., the radar SINR requirement. It demonstrates that double active RISs can more effectively reduce the interference from communication systems to radar compared with other schemes, and thus can improve the detection performance of the radar.

H. The Impact of Power Allocation Factor γ

In Fig. 8, we investigate the achievable data rate versus power allocation factor, i.e., γ. It can be seen that when $\gamma \leq 0.2$, all the schemes fail to find a feasible solution. As γ increases, double active RIS-assisted system is the first scheme to find a feasible solution compared with the other schemes, which means that the double active RISs-assisted RCC system only requires a low radar power budget, i.e., a small value of γ, to satisfy the radar detection performance, i.e., minimum SINR requirement. This is because that the double active RIS-assisted RCC system can well suppress the interference from the communication system to the radar. Furthermore, in the double active RIS-assisted RCC system, radar SINR requirements can be satisfied by assigning less power to the radar under a specified total power budget. Consequently, more

power can be allocated to double RISs and BS to enhance the achievable data rate.

VI. Conclusion

In this paper, we investigated the jointly beamforming design for a double active RIS-assisted RCC system. We formulated an achievable data rate maximization problem with the guaranteed radar SINR requirement and the power budget limitations of the radar and two active RISs. Because of the nonconvexity of the original problem, we proposed the PDD algorithm based on the FP method and CCP method to convert the original problem to a convex problem. In the inner loop of the PDD framework, we used the BCD method to divide the original problem into several subproblems. Then, we solved the subproblems using the Lagrange dual method. In the outer loop, we updated the dual variables and penalty factor. Simulation results verified the effectiveness of the proposed scheme. We also validated that the proposed algorithm based on the double active RIS-assisted system achieves better system performance than other benchmark schemes under the same power budget and number of reflecting elements. Furthermore, it is shown that double active RIS-assisted system has superior performance over other schemes in all locations of RISs.

For simplicity, self-interference between the two active RISs was not considered in this paper, and thus the effect of self-interference on RCC system will be further explored in future research work.

References

[1] X. You, C.-X. Wang et al., "Towards 6G wireless communication networks: Vision, enabling technologies, and new paradigm shifts," *Sci. China Inf. Sci.*, vol. 64, pp. 1–74, Nov. 2021.

[2] F. Liu et al., "Integrated sensing and communications: Toward dual-functional wireless networks for 6G and beyond," *IEEE J. Sel. Areas Commun.*, vol. 40, no. 6, pp. 1728–1767, Jun. 2022.

[3] A. Liu et al., "A survey on fundamental limits of integrated sensing and communication," *IEEE Commun. Surveys Tuts.*, vol. 24, no. 2, pp. 994–1034, 2nd Quar. 2022.

[4] F. Liu, C. Masouros et al., "Joint radar and communication design: Applications, state-of-the-art, and the road ahead," *IEEE Trans. Commun.*, vol. 68, no. 6, pp. 3834–3862, Jun. 2020.

[5] M. Labib, V. Marojevic, A. F. Martone, J. H. Reed, and A. I. Zaghloui, "Coexistence between communications and radar systems: A survey," *URSI Radio Sci. Bull.*, vol. 2017, no. 362, pp. 74–82, 2017.

[6] L. Zheng, M. Lops, Y. C. Eldar, and X. Wang, "Radar and communication coexistence: An overview: A review of recent methods," *IEEE Signal Process. Mag.*, vol. 36, no. 5, pp. 85–99, Sep. 2019.

[7] B. Li, A. P. Petropulu, and W. Trappe, "Optimum co-design for spectrum sharing between matrix completion based MIMO radars and a MIMO communication system," *IEEE Trans. Signal Process.*, vol. 64, no. 17, pp. 4562–4575, Sep. 2016.

[8] F. Liu, C. Masouros, A. Li, T. Ratnarajah, and J. Zhou, "MIMO radar and cellular coexistence: A power-efficient approach enabled by interference exploitation," *IEEE Trans. Signal Process.*, vol. 66, no. 14, pp. 3681–3695, Jul. 2018.

[9] R. Liu, M. Li, H. Luo, Q. Liu, and A. L. Swindlehurst, "Integrated sensing and communication with reconfigurable intelligent surfaces: Opportunities, applications, and future directions," *IEEE Wireless Commun.*, vol. 30, no. 1, pp. 50–57, Feb. 2023.

[10] C. Pan, G. Zhou, K. Zhi et al., "An overview of signal processing techniques for RIS/IRS-aided wireless systems," *IEEE J. Sel. Topics Signal Process.*, Aug. 2022.

[11] C. Pan et al., "Multicell MIMO communications relying on intelligent reflecting surfaces," *IEEE Trans. Wireless Commun.*, vol. 19, no. 8, pp. 5218–5233, Aug. 2020.

[12] Q. Wu and R. Zhang, "Intelligent reflecting surface enhanced wireless network via joint active and passive beamforming," *IEEE Trans. Wireless Commun.*, vol. 18, no. 11, pp. 5394–5409, Nov. 2019.

[13] X. Wang, Z. Fei, J. Guo, Z. Zheng, and B. Li, "RIS-assisted spectrum sharing between MIMO radar and MU-MISO communication systems," *IEEE Wireless Commun. Lett.*, vol. 10, no. 3, pp. 594–598, Mar. 2020.

[14] E. Shtaiwi, H. Zhang, A. Abdelhadi, A. L. Swindlehurst, Z. Han, and H. V. Poor, "Sum-rate maximization for RIS-assisted integrated sensing and communication systems with manifold optimization," *IEEE Trans. Commun.*, vol. 71, no. 8, pp. 4909–4923, Aug. 2023.

[15] Y. He, Y. Cai, H. Mao, and G. Yu, "RIS-assisted communication radar coexistence: Joint beamforming design and analysis," *IEEE J. Sel. Areas Commun.*, vol. 40, no. 7, pp. 2131–2145, Jul. 2022.

[16] Q. Wu, S. Zhang, B. Zheng, C. You, and R. Zhang, "Intelligent reflecting surface-aided wireless communications: A tutorial," *IEEE Trans. Commun.*, vol. 69, no. 5, pp. 3313–3351, May 2021.

[17] E. Björnson, Ö. Özdogan, and E. G. Larsson, "Intelligent reflecting surface versus decode-and-forward: How large surfaces are needed to beat relaying?" *IEEE Wireless Commun. Lett.*, vol. 9, no. 2, pp. 244–248, Feb. 2019.

[18] Z. Zhang et al., "Active RIS vs. passive RIS: Which will prevail in 6G?" *IEEE Trans. Commun.*, vol. 71, no. 3, pp. 1707–1725, Mar. 2022.

[19] Y. Sun et al., "Active-passive cascaded RIS-aided receiver design for jamming Nulling and signal enhancing," *IEEE Trans. Wireless Commun.*, pp. 1–1, 2023.

[20] G. Zhou et al., "A framework for transmission design for active RIS-aided communication with partial CSI," *IEEE Trans. Wireless Commun.*, 2023.

[21] K. Zhi, C. Pan, H. Ren, K. K. Chai, and M. Elkashlan, "Active RIS versus passive RIS: Which is superior with the same power budget?" *IEEE Commun. Lett.*, vol. 26, no. 5, pp. 1150–1154, May 2022.

[22] Z. Yu et al., "Active RIS-aided ISAC systems: Beamforming design and performance analysis," *IEEE Trans. Commun.*, vol. 72, no. 3, pp. 1578–1595, Mar. 2024.

[23] Y. Zhang, J. Chen, C. Zhong, H. Peng, and W. Lu, "active IRS-assisted integrated sensing and communication in C-RAN," *IEEE Wireless Commun. Lett.*, vol. 12, no. 3, pp. 411–415, Mar. 2023.

[24] A. A. Salem, M. H. Ismail, and A. S. Ibrahim, "Active reconfigurable intelligent surface-assisted MISO integrated sensing and communication systems for secure operation," *IEEE Trans. Veh. Technol.*, Apr. 2022.

[25] A. L. Swindlehurst, G. Zhou, R. Liu, C. Pan, and M. Li, "Channel estimation with reconfigurable intelligent surfaces—a general framework," *Proc. IEEE*, vol. 110, no. 9, pp. 1312–1338, Sep. 2022.

[26] B. Zheng, C. You, and R. Zhang, "Efficient channel estimation for double-IRS aided multi-user MIMO system," *IEEE Trans. Commun.*, vol. 69, no. 6, pp. 3818–3832, Jun. 2021.

[27] K. K. Kishor and S. V. Hum, "An amplifying reconfigurable reflectarray antenna," *IEEE Trans. Antennas Propag.*, vol. 60, no. 1, pp. 197–205, Jan. 2012.

[28] J.-F. Bousquet, S. Magierowski, and G. G. Messier, "A 4-GHz active scatterer in 130-nm CMOS for phase sweep amplify-and-forward," *IEEE Trans. Circuits Syst. I*, vol. 59, no. 3, pp. 529–540, Mar. 2012.

[29] B. Li and A. Petropulu, "MIMO radar and communication spectrum sharing with clutter mitigation," in *Proc. IEEE Radar Conf. (RadarConf)*, May 2016, pp. 1–6.

[30] L. Zheng, M. Lops, and X. Wang, "Adaptive interference removal for uncoordinated radar/communication coexistence," *IEEE J. Sel. Topics Signal Process.*, vol. 12, no. 1, pp. 45–60, Feb. 2017.

[31] A. Khawar, A. Abdel-Hadi, and T. C. Clancy, "Spectrum sharing between S-band radar and LTE cellular system: A spatial approach," in *Proc. IEEE Int. Symp. Dynamic Spectr. Access Netw. (DYSPAN)*. IEEE, Apr. 2014, pp. 7–14.

[32] K. Shen and W. Yu, "Fractional programming for communication systems—part i: Power control and beamforming," *IEEE Trans. Signal Process.*, vol. 66, no. 10, pp. 2616–2630, May 2018.

[33] Q. Shi and M. Hong, "Penalty dual decomposition method for nonsmooth nonconvex optimization—part i: Algorithms and convergence analysis," *IEEE Trans. Signal Process.*, vol. 68, pp. 4108–4122, Jun. 2020.

[34] A. L. Yuille and A. Rangarajan, "The concave-convex procedure," *Neural Comput.*, vol. 15, no. 4, pp. 915–936, 2003.

[35] M. Grant and S. Boyd, "CVX: Matlab software for disciplined convex programming, version 2.1," 2014.

[36] D. P. Bertsekas, "Nonlinear programming," *J. Oper. Res. Soc.*, vol. 48, no. 3, pp. 334–334, 1997.

[37] S. Boyd, N. Parikh, E. Chu, B. Peleato, J. Eckstein et al., "Distributed optimization and statistical learning via the alternating direction method of multipliers," *Foundations Trends Mach. Learn.*, vol. 3, no. 1, pp. 1–122, 2011.
[38] X.-D. Zhang, *Matrix analysis and applications*. Cambridge Univ. Press, 2017.
[39] S. Boyd and Z. Luo, "EE392o: Optimization projects," Available: [Online]. Available: http://www.stanford.edu/class/ee392o, 2004.
[40] Y. Sun, P. Babu, and D. P. Palomar, "Majorization-minimization algorithms in signal processing, communications, and machine learning," *IEEE Trans. Signal Process.*, vol. 65, no. 3, pp. 794–816, 2016.
[41] B. Zheng, C. You, and R. Zhang, "Double-IRS assisted multi-user MIMO: Cooperative passive beamforming design," *IEEE Trans. Wireless Commun.*, vol. 20, no. 7, pp. 4513–4526, Jul. 2021.

Mengyu Liu received the B.E. degree from the School of Electronic and Information Engineering, Beijing Jiaotong University, Beijing, China, in 2023. He is currently pursuing the M.E. degree with the School of Information Science and Engineering, Southeast University, Nanjing, China. His research interests include massive MIMO, reconfigurable intelligent surfaces, and near-field communications.

Hong Ren (Member, IEEE) received the B.S. degree in electrical engineering from Southwest Jiaotong University, Chengdu, China, in 2011, and the M.S. and Ph.D. degrees in electrical engineering from Southeast University, Nanjing, China, in 2014 and 2018, respectively. From 2016 to 2018, she was a visiting student with the School of Electronics and Computer Science, University of Southampton, U.K. From 2018 to 2020, she was a Postdoctoral Scholar with the Queen Mary University of London, U.K. She is currently an Associate Professor with Southeast University. Her research interests lie in the areas of communication and signal processing, including cooperative ISAC, machine learning, and URLLC. She was a recipient of the 2024 lEEE Communications Society Fred WEllersick Prize and the 2022 lEEE Communications Society Leonard G. AbrahamPrize.

Cunhua Pan (Senior Member, IEEE) is a Full Professor with Southeast University. He has published over 200 IEEE journal papers. His papers got over 16,000 Google Scholar citations with H-index of 63. His research interests mainly include reconfigurable intelligent surfaces, AI for Wireless, and near field communications and sensing. He received the IEEE ComSoc Leonard G. Abraham Prize in 2022, the IEEE ComSoc Asia-Pacific Outstanding Young Researcher Award in 2022, and the IEEE ComSoc Fred W. Ellersick Prize in 2024. He is a Clarivate Highly Cited researcher. He is/was an Editor of IEEE TRANSACTION ON COMMUNICATIONS, IEEE TRANSACTIONS ON VEHICULAR TECHNOLOGY, IEEE WIRELESS COMMUNICATION LETTERS, IEEE COMMUNICATIONS LETTERS, and IEEE ACCESS. He serves as a Guest Editor for IEEE JOURNAL ON SELECTED AREAS IN COMMUNICATIONS on the special issue on xURLLC in 6G: Next Generation Ultra-Reliable and Low-Latency Communications. He also serves as a Leading Guest Editor of IEEE JOURNAL OF SELECTED TOPICS IN SIGNAL PROCESSING Special Issue on Advanced Signal Processing for Reconfigurable Intelligent Surface-Aided 6G Networks, for *IEEE Vehicular Technology Magazine* on the Special Issue on Backscatter and Reconfigurable Intelligent Surface Empowered Wireless Communications in 6G, for IEEE OPEN JOURNAL OF VEHICULAR TECHNOLOGY on the Special Issue of Reconfigurable Intelligent Surface Empowered Wireless Communications in 6G and Beyond, and for IEEE TRANSACTIONS ON GREEN COMMUNICATIONS AND NETWORKING Special Issue on Design of Green Near-Field Wireless Communication Networks.

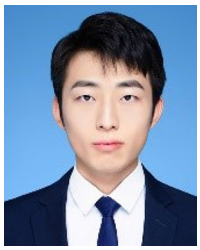

Boshi Wang received the B.S. degree from the School of Information Science and Engineering, Southeast University, Nanjing, China, in 2023, where he is currently pursuing the master's degree. His research interests include reconfigurable intelligent surfaces.

Zhiyuan Yu received the B.S. degree from the School of Information Science and Engineering, Southeast University, Nanjing, China, in 2023, where he is currently pursuing the master's degree. His research interests include reconfigurable intelligent surfaces, and integrated sensing and communication.

Ruisong Weng received the B.E. degree from the Software Institute, Nanjing University, Nanjing, China, in 2020, and the M.E. degree from the College of Information, Mechanical and Electrical Engineering, Shanghai Normal University, Shanghai, China, in 2023. He is currently pursuing the Ph.D. degree with the School of Information Science and Engineering, Southeast University, Nanjing. His major research interests include reconfigurable intelligent surface, and channel estimation and signal processing.

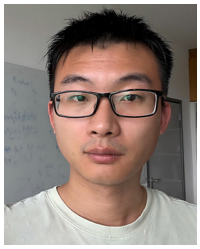

Kangda Zhi received the B.Eng. degree from the School of Communication and Information Engineering, Shanghai University, Shanghai, China, in 2017, the M.Eng. degree from School of Information Science and Technology, University of Science and Technology of China, Hefei, China, in 2020, and the Ph.D. degree from the School of Electronic Engineering and Computer Science, Queen Mary University of London, U.K., in 2023. He is currently a Postdoctoral Researcher with the School of Electrical Engineering and Computer Science, Technical University of Berlin, Germany. His research interests include reconfigurable intelligent surface, massive MIMO, and near-field communications. He received the Exemplary Reviewer Certificate of the IEEE WIRELESS COMMUNICATIONS LETTERS in 2021 and 2022, and the IEEE COMMUNICATIONS LETTERS in 2023.

Yongchao He received the B.S. degree from the School of Communication and Information Engineering, Nanjing University of Posts and Telecommunications in 2023. He is currently pursuing the master's degree with Southeast University, Nanjing, China. His research interests include reconfigurable smart surfaces, and 5G new radio link-level simulation.